ABSTRACT

Title of Document:	THE EFFECT OF PACKAGE GEOMETRY ON MOISTURE-DRIVEN DEGRADATION OF POLYMER ALUMINUM CAPACITORS
	Helmut Manfred Bevensee, Master of Science, May 2016
Directed By:	Assistant Research Scientist, Michael H. Azarian, Center for Advanced Life Cycle Engineering

Polymer aluminum electrolytic capacitors were introduced to provide an alternative to liquid electrolytic capacitors. Polymer electrolytic capacitor electric parameters of capacitance and ESR are less temperature dependent than those of liquid aluminum electrolytic capacitors. Furthermore, the electrical conductivity of the polymer used in these capacitors (poly-3,4ethylenedioxithiophene) is orders of magnitude higher than the electrolytes used in liquid aluminum electrolytic capacitors, resulting in capacitors with much lower equivalent series resistance which are suitable for use in high ripple-current applications. The presence of the moisture-sensitive polymer PEDOT introduces concerns on the reliability of polymer aluminum capacitors in high humidity conditions. Highly accelerated stress testing (or HAST) (110ºC, 85% relative humidity) of polymer aluminum capacitors in which the parts were subjected to unbiased HAST conditions for 700 hours was done to understand the design factors that contribute to the susceptibility to degradation of a polymer

aluminum electrolytic capacitor exposed to HAST conditions. A large scale study involving capacitors of different electrical ratings (2.5V – 16V, 100µF – 470 µF), mounting types (surface-mount and through-hole) and manufacturers (6 different manufacturers) was done to determine a relationship between package geometry and reliability in high temperature-humidity conditions. A Geometry-Based HAST test in which the part selection limited variations between capacitor samples to geometric differences only was done to analyze the effect of package geometry on humidity-driven degradation more closely. Raman spectroscopy, x-ray imaging, environmental scanning electron microscopy, and destructive analysis of the capacitors after HAST exposure was done to determine the failure mechanisms of polymer aluminum capacitors under high temperature-humidity conditions.

THE EFFECT OF PACKAGE GEOMETRY ON MOISTURE-DRIVEN DEGRADATION OF POLYMER ALUMINUM CAPACITORS

by

Helmut Manfred Bevensee

Thesis submitted to the Faculty of the Graduate School of the
University of Maryland, College Park, in partial fulfillment
of the requirements for the degree of
Master of Science
2016

Advisory Committee:
Assistant Research Scientist Michael H. Azarian, Chair
Professor Michael Pecht
Professor F. Patrick McCluskey
Professor Peter Sandborn

Dedication

This thesis is dedicated to my parents, Erich and Ana, for being the best role models a son could ask for, and for the sacrifices you have made to provide me with all the opportunities I've been lucky to have. I would not be where I am today if it were not for my father being the engineer I aspire to be, and my mother's constant support and encouragement throughout my studies.

I would also like to dedicate my thesis to my girlfriend Lauren, who has been by my side for a better part of the last 5 years, and has been providing me with constant support as we both work towards our goals and aspirations.

Acknowledgements

I would like to start by thanking my advisor Dr. Michael H. Azarian, Dr. Diganta Das, and Professor Michael Pecht for giving me an opportunity to be a part of the Center for Advanced Life Cycle Engineering at the University of Maryland as a graduate research assistant in order to further my education and get my Master's degree. I would like to thank Dr. Michael H. Azarian for his support, guidance, suggestions and encouragement as I completed my master's thesis research.

I would also like to thank Professor Michael Pecht, Professor F. Patrick McCluskey and Professor Peter Sandborn for taking the time to be in my master's thesis committee and their helpful feedback and recommendations.

Thanks are also in order for the professors, research faculty, and students who attended my research update presentation and provided the valuable feedback necessary to move forward with my research. Those individuals especially include Dr. Michael H. Azarian, Dr. Diganta Das, Dr. Carlos Morillo, Anto Peter, and Jordan Jameson and more. Special thanks are also in order to Dr. Karen Gaskell at the chemistry department for taking the time to explain and help me with Raman spectroscopy, which played a large role in my thesis work.

Table of Contents

List of Tables

List of Figures

List of Abbreviations

ESR – Equivalent Series Resistance

LC – Leakage Current

DF – Dissipation Factor

EDOT - 3,4-ethylenedioxythiophene

PEDOT – Poly,3,4-ethylenedioxythiophene

HAST – Highly accelerated stress testing

Chapter 1: Introduction: Aluminum Electrolytic Capacitors

1.1 Aluminum Electrolytic Capacitors

The origin of electrolytic capacitors dates back to the late 1800's, when the first type of liquid electrolytic capacitor was developed [1].These capacitors consist of an aluminum anode, an aluminum oxide dielectric, and a cathode consisting of a liquid electrolyte and a metal such as aluminum. Since then, liquid electrolytic capacitors have not changed much in their basic structure. Electrolytic capacitors serve a range of capacitance values from 1 to 100,000 μF, and rated voltages of up to 600V. Generally, applications for electrolytic capacitors include filtering in DC circuits, rectified circuits, pulsing circuits such as strobe lights, and silicon controlled rectifier communication circuits [2].

Aluminum electrolytic capacitors are able to achieve high capacitance densities through the use of a highly etched aluminum anode foil, which increases the surface area of the capacitor by up to 150 times [1]. In order to increase the contact area between the dielectric and the cathode of the capacitor, a conducting liquid electrolyte has been traditionally used to improve the contact area between the highly etched dielectric and

cathode aluminum foil. This effectively extends the cathode of the capacitor to include the liquid electrolyte, as can be seen in **Figure *1***.

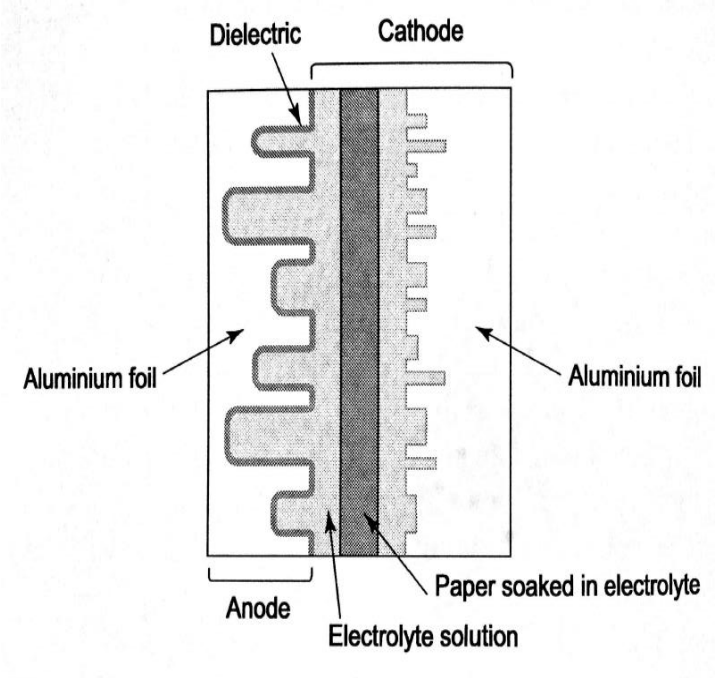

Figure 1. Representation of an Aluminum Electrolytic Capacitor Element *[1]*

Although electrolytic capacitors have been able to achieve high capacitance densities and high voltages, they are known for their high equivalent series resistance and dissipation factor, which are associated to high energy losses [1] [2]. The equivalent series resistance of these capacitors can be in large part attributed to the resistivity of their electrolyte materials, which can be orders of magnitude higher than the metallic parts of the anode and cathode foils. For example, the conductivity of aluminum is around $3.50\times10^{\wedge5}$ S/cm, while the conductivity of an electrolyte can be around 0.01 S/cm [3]. Lower equivalent series values can thus be achieved by using electrolytes with higher conductivities. The development of new conducting materials with higher conductivities in the last century have led to the development of capacitors with lower losses. One such

candidate material to replace liquid electrolytes is Poly,3,4-ethylenedioxythiophene, also known as PEDOT, which has been shown to achieve conductivities as high as 1000 S/cm [4].

PEDOT is a π-conjugated conducting polymer based on the monomer 3,4-ethylenedioxythiophene (EDOT) developed by Bayer AG in 1988 [4]. Today, PEDOT is the most commonly used conducting polymer in polymer aluminum electrolytic capacitors [4] [5]. Intrinsically conducting polymers become conducting by removing an electron from their conjugated π-orbitals via doping which results in the delocalization of electrons along the polymer backbone [4]. The polymer is synthesized when the monomer EDOT is put in a solution containing an oxidant, which polymerizes EDOT and subsequently dopes PEDOT [4] [6] [7].

Today's conventional aluminum electrolytic capacitors use a wound capacitor element structure encased in an aluminum can. The capacitor element (represented in **Figure *1***) of an electrolytic capacitor consists of an anode aluminum foil, a layer of aluminum oxide, an electrolyte (or polymer)-impregnated paper separator, and a cathode

aluminum foil. A scanning electron microscope image of a cross section showing the different components of a polymer aluminum capacitor element are shown in **Figure *2***.

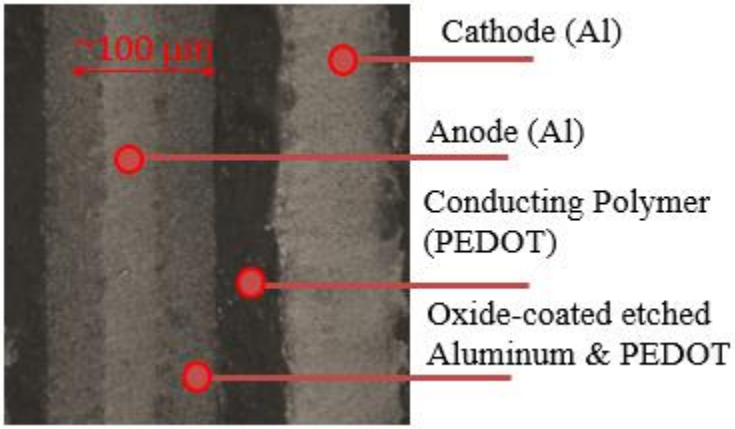

Figure 2. Cross Sectional View of Polymer Aluminum Capacitor Element

The anode foil is coated in a thin, dense, and non-porous barrier layer of Al_2O_3 which acts as the dielectric [8]. This capacitor element is encased in an aluminum can and then sealed with a rubber bung. The two leads extending out of the capacitor element pass through punctures on the rubber bung. The aluminum can is then crimped around the rubber bung to complete the seal. A schematic illustrating the different parts that make up these capacitors is shown in Figure 3.

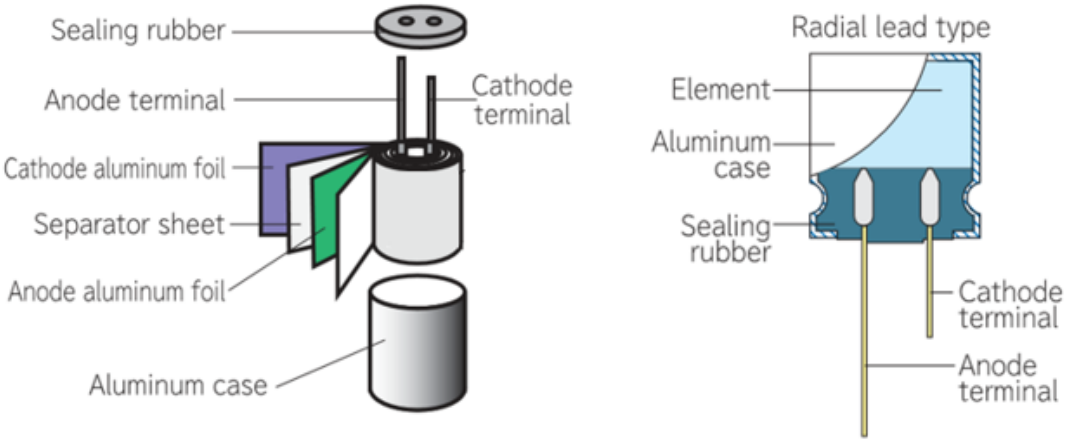

Figure 3. Schematic of Aluminum Electrolytic Capacitor *[9]*

1.2 Polymer Aluminum Capacitors

Aluminum electrolytic capacitors of the wound type that use a conducting polymer as the cathode are almost identical in structure to their liquid electrolyte predecessors. The main difference between aluminum liquid electrolytic capacitors and polymer aluminum capacitors of the wound structure is the material of the electrolyte. While liquid aluminum electrolytic capacitors use a liquid electrolyte, polymer aluminum electrolytic capacitors use the conducting polymer PEDOT. The majority of applications of polymer aluminum capacitors are associated with computer motherboards, power supply supplies, high end graphics card production, digital cameras, and flat panel displays [10]. More specifically, uses for these capacitors include backup current for integrated circuits, bypass of signal noise, low-pass filtering, and input-output smoothing in converters [11].

1.3 Advantages of Polymer Aluminum Electrolytic Capacitors

Polymer aluminum capacitors have several advantages over competing capacitor technologies. Since the only noticeable difference between liquid and polymer aluminum capacitors is in the electrolyte material, these advantages are related to the elimination of the liquid electrolyte.

The first and most important advantage of polymer aluminum capacitors over liquid electrolytic capacitors is their low equivalent series resistance (ESR) and dissipation factor. While work at CALCE has shown liquid electrolytic capacitors with ESR values as low as ~ 40 mΩ, polymer aluminum capacitors are often rated for ESR values around 5-15 mΩ. Furthermore, electrical characterization work of polymer aluminum capacitors by NASA in 2009 shows that polymer aluminum capacitors demonstrate performance over MnO_2 – based and polymer based tantalum capacitors with extremely low ESR [12]. Lower ESR

values can diminish the number of capacitors required in a circuit and thus lower costs and space requirements [13].

The material selection and construction of polymer aluminum capacitors leads to benign failures which occur gradually in the form of drifts in electrical parameters over time (wear out), as opposed to catastrophic failures that are a result of overstress. The electrical characterization work by NASA demonstrated that polymer aluminum electrolytic capacitors exhibit ignition-free and non-flammable failure modes when subjected to reverse bias and over-stress conditions [12]. This is an advantage over tantalum capacitors which can enter thermal runaway when exposed to surge currents or voltage over-stress [14]. Benign failures in polymer aluminum capacitors are also an advantage of liquid aluminum electrolytic capacitors which are known to explode in overstress conditions due to internal heating and vaporization of the electrolyte [15].

Temperature stability of polymer aluminum capacitors is also considered an advantage over their liquid electrolyte counterparts. The temperature-dependent electrical characteristics of liquid electrolytes result in capacitors with temperature-dependent electrical parameters. More specifically, liquid electrolytic capacitors show changes in capacitance and ESR over their rated temperature range. This is due to a decrease in conductivity of the liquid electrolyte and increase in viscosity in low temperatures, leading to increased ESR and decreased capacitance. Since the conductivity of the polymer PEDOT is constant over the capacitor's rated operating temperatures
(-55ºC to around 105ºC), polymer aluminum capacitors show much more stable ESR over that temperature range, as seen in Figure 4 [9].

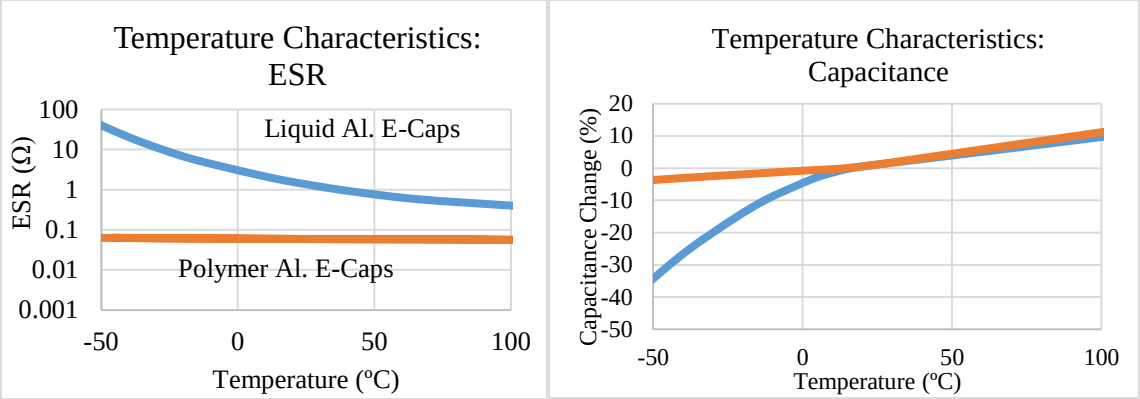

Figure 4. Temperature Characteristics of Liquid and Polymer Aluminum Electrolytic Capacitors. (Adapted from *[9]*)

1.4 Construction of Polymer Aluminum Capacitors

One of the defining features of polymer aluminum capacitors and aluminum electrolytic capacitors are the highly etched anode aluminum foils used to achieve high surface area and consequently high capacitance densities. Another one of the defining features is the use of a very thin electrochemically formed aluminum oxide layer that functions as the dielectric. This highly etched structure of aluminum and aluminum oxide requires a conducting material that can form a good electrical connection between the anode and cathode foils.

The unique capacitor structure of polymer aluminum capacitors is achieved through a series of manufacturing steps. The first step in the production of these capacitors is the etching of the aluminum foil. This is done by anodic dissolution of aluminum in hot chloride solutions which produces a high density of etched tunnels [16]. A cross sectional image of an etched aluminum foil is shown in **Figure *5***.

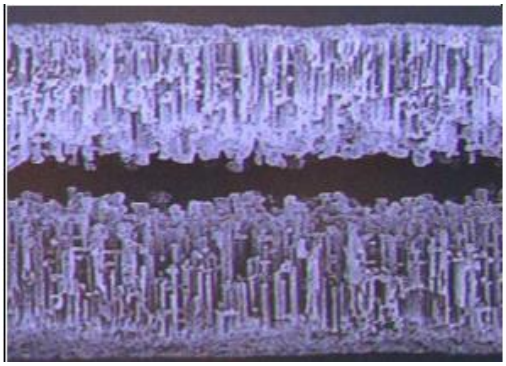

Figure 5. Etched Anode Foil Prior to Dielectric Forming *[8]*

This process can result in increases of surface area of the aluminum foil of up to 150 times [8]. The next step in the manufacture of these capacitors is the formation of the dielectric layer composed of alumina on the etched aluminum anode. This is done by immersing the etched aluminum into a solution containing an ammonium salt of boric or phosphoric acid and applying a DC voltage to the aluminum. This results in an oxide formation with a thickness dependent on the DC voltage (or forming voltage) applied to the aluminum. The thicknes achieved by the forming voltage is in the order of 1.3 to 1.5 nanometers per volt applied [17]. This method results in a dense, non-porous, barrier-type aluminum oxide. A schematic showing how the dielectric coats the highly etched aluminum anode is shown in **Figure *6***. An optical microscope image of what is represented in **Figure *6*** is shown in **Figure *7***

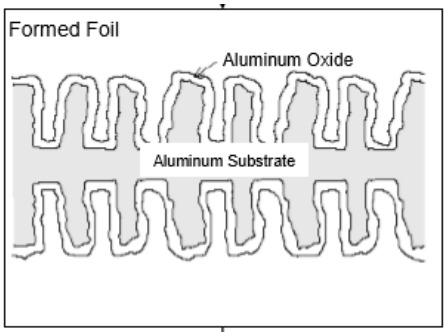

Figure 6. Schematic of Anodic Oxide *[8]*

Figure 7. Cross Section of Anode Foil with Oxide-Covered Etched Aluminum

The next step in the manufacturing process is the slitting process, in which the master sheets of foil that have been etched and formed are cut into thinner strips as specified by the part geometric specifications. The strips are then stitched with lead tabs and wound into a cylindrical element. A paper separator is used between the anode and cathode foils [8] [9]. After this step comes the application of the polymer PEDOT to the capacitor element. This is done by chemical in-situ polymerization of a monomer with an oxidizer [4]. This is typically done by first dipping the capacitor element into an oxidizer solution. The solvent must then be evaporated in order to dip the capacitor element into a solution of the monomer EDOT [4]. Once the polymerization process is completed, the capacitor element is placed in an aluminum can, sealed using a rubber bung, and the aluminum canned is crimped around the rubber bung to complete the seal. Finally, the capacitors are aged by being subjected to a DC voltage at high temperatures in order to repair any oxide that might have been damage during the manufacturing process.

1.5 Manufacturer-Stated Effect of Moisture on Polymer Aluminum Electrolytic Capacitors

Although polymer aluminum electrolytic capacitors have their clear advantages over other capacitor technologies, manufacturers often include warnings against storing or subjecting these capacitors to humid conditions. A conference paper by Rapoza et. al from capacitor manufacturer Cornell Dubilier states that ambient temperature and relative humidity affect the life of polymer aluminum capacitors, with a reduction in humidity

having the greatest effect on extending the life expected life [18]. Another major capacitor manufacturer Murata states in their application notes that polymer aluminum capacitors should be stored at temperatures between 5-30ºC and less than 60% relative humidity [19]. Capacitor manufacturer Vishay states in their technical notes that polymer aluminum capacitors should not be stored in high-humidity conditions over 75% relative humidity [20]. Manufacturer X-CON advises that storage in high-humidity environments will lead to an increase in leakage current [21].

The susceptibility of these capacitors to degradation in high-humidity environments is well-documented in manufacturer application notes and technical guidelines. Although manufacturers point out the susceptibility of these capacitors to degradation in high-humidity, a detailed explanation on the failure/degradation mechanisms associated with humidity is not provided by manufacturers. Furthermore, without extensive knowledge about the failure\degradation mechanisms of polymer aluminum capacitors in humid conditions, it is difficult to determine what features make one capacitor more robust to humidity than another capacitor. The following literature review is intended to explore any work that has been done to understand the factors that contribute to degradation in polymer aluminum capacitors in an effort to understand why and how humidity is causing these capacitors to degrade.

1.6 Literature Review

Polymer aluminum capacitors are a relatively new technology, with the first polymer aluminum capacitors emerging sometime around 1995 [10]. Since the inception of this new capacitor technology, few studies have been done to understand the factors that contribute to degradation. This literature review will cover studies that have been done on

polymer aluminum capacitors directly, as well as studies on the effect of humidity on the conducting polymer PEDOT, which is used in these polymer aluminum capacitors.

Electrical characterization of polymer aluminum capacitors was done by NASA in a report published in 2009 in which the polymer aluminum capacitors were compared to polymer tantalum and manganese dioxide tantalum capacitors [12]. After initial electrical characterization, which demonstrated lower ESR values for polymer aluminum capacitors than tantalum capacitors, test capacitors were subjected to reverse voltages twice the amount of their rated values. The objective of the reverse voltage was to serve as a "push-to-failure" type test and learn of the failure modes of polymer aluminum capacitors. Results showed that all manganese dioxide tantalum experienced sustained combustion, while all the polymer aluminum capacitors did not show any sign of combustion. Additionally, it was found that polymer aluminum capacitors had the best frequency and temperature characteristics in terms of ESR of any competing capacitor technology in the voltage ranges of less than 6.3V. Finally, these capacitors were exposed to thermal vacuum tests of cycles between -55°C and +105°C at 10^{-5} Torr and showed no impact on electrical characteristics of these capacitors. In order to space-rate polymer aluminum capacitors, the NASA report cites 85°C/85% relative humidity testing of polymer aluminum capacitors among other tests as one of the next item on their to-do list.

A study published in 2013 by Kim et al. titled studied the effects that different oxidants have on the performance of polymer aluminum capacitors [6]. Polymer aluminum capacitors with benzenesulfonate-doped poly(3,4- ethylenedioxythiophene) (PEDOT-OBs), 4-methyl-benzenesulfonate-doped poly(3,4- ethylenedioxythiophene) (PEDOT-OMBs) and 4-ethyl-benzenesulfonate-doped poly(3,4- ethylenedioxythiophene) (PEDOT-

OEBs) were fabricated and their electrical properties were compared. What Kim et al. found was that the various types of PEDOT that were doped with separate oxidants had different levels of doping. Doping levels of 34.9% were observed for PEDOT-OBs, 31.5% for PEDOT-OMBs, and 29.3% for PEDOT-OEBs. Consequently, improved electrical characteristics of capacitance, ESR, and leakage current were seen with increasing doping levels. The importance of doping level and capacitor performance lies in the fact that undoped oxidants can potentially react with hydroxyl groups and/or absorbed water resulting in acid formation which can dissolve the dielectric layer. While aluminum oxide tends to form in most conditions, the presence of salt solutions with high or low pH values has been known to dissolve aluminum oxide [17]. Furthermore, higher doping levels are associated with higher conductivities in PEDOT because unreacted oxidants in the polymer matrix increase its resistance.

The relationship of reduced ESR with increased doping level is attributed to two factors; an increase in conductivity (and reduction of resistance) of a polymer with increasing doping level, and a decrease in resistance due to improved contact area of the polymer and aluminum oxide dielectric of the capacitor. The increase in capacitance for capacitors with higher doping levels can be attributed to the lesser amount of damage to the dielectric/polymer surface area caused by the formation of acid solutions harmful to the dielectric. The concentrations of these acids at the interface increase with decreased doping levels. Finally, the increase in leakage current in capacitors with lower doping levels can also be attributed to damage to the dielectric from acid formation.

A separate study to show the effect of damage to the polymer/dielectric interface on polymer aluminum capacitors was done by Nogami et al. in 2007 [7]. Polymer

aluminum capacitors of the wound structure were fabricated using p-toluenesulfonate-doped poly(3,4- ethylenedioxythiophene) (PEDOT-PTs). By coating the dielectric surface with an extremely thin layer of hyperbranched Poly(solixysilane)s (HBPSi), Nogami et al. were able to reduce the amount of damage to the dielectric/polymer interface that would arise from the formation of acids which are a product of the reaction of absorbed moisture with undoped oxidants. Results shown reported reduced ESR and leakage current on capacitors fabricated with the thin HBPSi coating on the dielectric versus conventional capacitors. **Figure *8*** shows a schematic indicating where the HBPSI-coated aluminum oxide layer is located in relation to the aluminum anode and polymer.

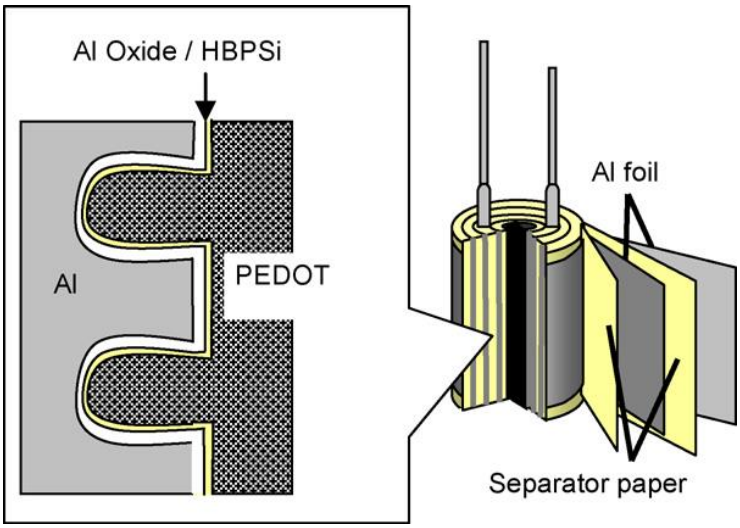

Figure 8. Schematic of polymer aluminum capacitor with protective HBPSi *[7]*

While the last two studies focused in part on the effect that damage to the dielectric/polymer interface can have on these capacitors, the following papers discuss the changes in electrical conductivity of the polymer PEDOT in relation to humidity in the atmosphere.

Kus et al. performed a study titled “Electrical Characterization of PEDOT: PSS Beyond Humidity Saturation” in which a PEDOT: PSS humidity sensor was fabricated [22]. By subjecting the humidity sensor to varying relative humidity conditions, the authors were able to see reversible electrical properties of conductivity up to 80% relative humidity. As can be seen in **Figure 9**, the relationship between resistivity and relative humidity are linearly correlated up until a level of 80% relative humidity.

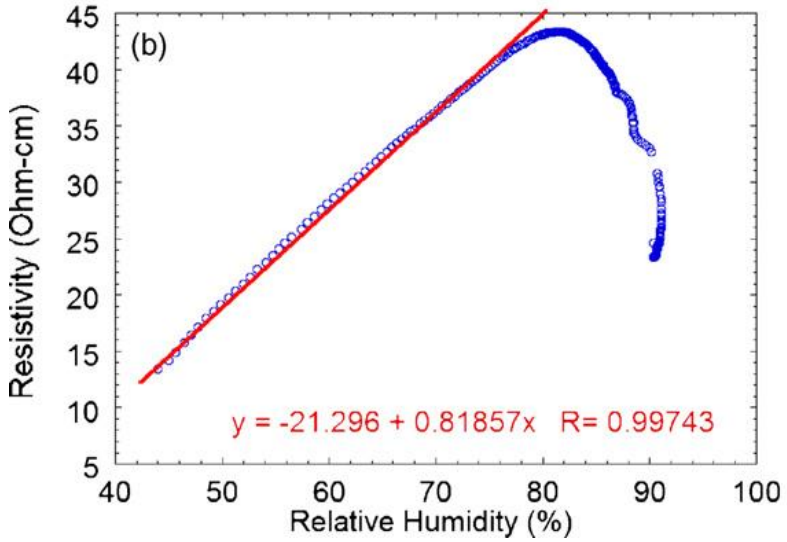

Figure 9. Humidity-Dependent Resistivity of PEDOT-Based Humidity Sensor *[22]*

Up until 80% relative humidity, the increase in resistivity was attributed to the increase in distance between PEDOT chains in the polymer matrix as a result of an increase in the presence of water molecules. The larger distance between PEDOT chains makes the conducting mechanism of electron hopping more difficult, therefore increasing the resistance of the polymer. The sharp decrease in resistivity past 80% relative humidity is attributed to the formation of a meniscus layer of water upon saturation of the polymer, which dissolves PSS protons and atmospheric gases, thus leading to an increase in ionic conductivity past the 80% relative humidity saturation point.

Another study done in 2005 by Kang et al. was done in which the humidity-dependent characteristics of a thin film PEDOT field-effect transistor (FET) were studied [23]. Using PEDOT in the gate and source-drain electrodes, and active channels of the device, the device characteristics were monitored in different humidity conditions ranging from 0% (in a vacuum) to 55% relative humidity. The result of the testing was a humidity-dependent FET, whose changing properties were attributed to changes of conductivity of in the PEDOT in humid conditions due to de-doping, although de-doping of the polymer was never directly observed but only speculated as an explanation for the change in characteristics of the polymer.

A ph.d thesis from the University of Maryland written by A. Shrivastava at the mechanical engineering department included elevated temperature-humidity testing of surface-mount and through-hole polymer aluminum capacitors from 2 different manufacturers at 85°C, 85% relative humidity (R.H.), and HAST testing at 110°C, 85% R.H. [24]. The failure modes for capacitors subjected to 85°C, 85% R.H. and 110°C, 85% R.H. conditions were identical, so HAST was deemed as a rapid assessment tool for polymer aluminum capacitors at elevated temperature-humidity conditions.

In summary, only a limited amount of work has been done to understand the factors that contribute to the degradation of these capacitors. Capacitor manufacturers often cite warnings and operating condition recommendations with little explanation behind the failure or degradation mechanisms of these capacitors. NASA only first started to do electrical characterizations of these capacitors in 2009, and no humidity-related studies have ever been published. It is surprising that no humidity studies on polymer aluminum capacitors have been published since humidity is a concern stated in all application notes

from different manufacturers. Furthermore, through studies focusing on damage at the dielectric/polymer interface, it has been shown that the residual oxidant material left over as a by-product of the in-situ chemical polymerization process can react with adsorbed moisture to create acid solutions that can damage the dielectric. These studies show that the interface at the polymer/dielectric interface is crucial to the performance of these capacitors and offers an explanation as to how moisture can play a role in damaging these capacitors through the formation of acid solutions. Furthermore, studies unrelated to polymer capacitors, but that instead look at the humidity-dependent characteristics of the polymer PEDOT suggest that absorption of moisture by the polymer has been shown to result in increases in resistivity of the polymer.

1.7 Research Objectives

The objectives of the research are to:

- Determine the role that package geometry plays in the susceptibility of polymer aluminum capacitors to degradation in HAST (110ºC, 85% R.H) conditions.
- Determine if de-doping of the conducting polymer in the presence of moisture is one of the degradation mechanisms of these capacitors.
- Determine the failure/degradation mechanisms seen in polymer aluminum capacitors subjected to HAST (110ºC, 85% R.H).

Chapter 2: Evaluation of Moisture-Driven Degradation of Polymer Aluminum Electrolytic Capacitors

2.1 Objectives

The objectives of subjecting polymer aluminum capacitors to HAST was to precipitate humidity-driven failures in the capacitor samples while also conducting dry heat testing to determine the amount of degradation seen in HAST testing that can be attributed to high temperature and humidity conditions versus high temperature conditions. The results of the HAST testing were used to learn about the factors, such as package geometry, that can affect the reliability of polymer aluminum capacitors in high humidity conditions. Furthermore, HAST testing of polymer aluminum capacitors yielded test samples that could then be analyzed and studied to determine the humidity-related failure or degradation mechanisms.

2.2 Experimental Approach

2.2.1 Test Conditions and Test Chambers

Test conditions for HAST follow JEDEC standard JESD22-A118 for unbiased HAST. HAST test conditions of 110ºC, 85% relative humidity, and 1.2 atm pressure were used for 2 separate HAST studies done. Dry heat test conditions of 110 ºC and unregulated relative humidity were also used. These tests were performed to achieve the goal of precipitating humidity-driven failures in polymer aluminum capacitors, as well as providing test results for capacitors used in dry heat conditions to show the effect that humidity has on polymer aluminum capacitors. The HAST chamber used for this testing

was an ESPEC TPC-212M HAST System, and the oven used for the dry heat exposure was a JEIO-Tech OF-22 forced convection oven.

2.2.2 Part Selection

Capacitors from different manufacturers were carefully selected to study the factors that contribute to the degradation of these capacitors in high humidity conditions. In order to understand these factor, HAST testing of polymer aluminum capacitors was split into two separate tests in which different part selection criteria were applied. The preliminary HAST test included capacitors that were both surface-mount and through-hole capacitors of a variety of capacitance, voltage ratings, shapes and sizes. Sample sizes of 20 capacitors from 16 different part numbers were chosen for this study for a total of test 320 capacitors. Table 1 and

Table *2* show the rated voltage, rated capacitance, manufacturer, and sample size of the capacitors selected for this HAST test.

Table 1. Surface Mount Capacitors for Preliminary HAST Test

Surface Mount				
Part	Capacitance (μF)	Rated Voltage (V)	Sample Size	Manufacturer
A	220	6.3	20	M1
B	330	2.5	20	M1
C	220	6.3	20	M2
D	330	2.5	20	M2
E	330	6.3	20	M3
F	220	6.3	20	M3
G	220	6.3	20	M4
H	330	2.5	20	M4

Table 2. Through-Hole Capacitors for Preliminary HAST Test

Through-Hole				
Part	Capacitance (μF)	Rated Voltage	Sample Size	Manufacturer
I	560	6.3	20	M5
J	560	6.3	20	M5
K	470	6.3	20	M5
L	470	6.3	20	M5
M	270	16	20	M5
N	560	6.3	20	M1
O	100	6.3	20	M1
P	470	6.3	20	M1

The part selection for the Geometry-Based HAST test does not include capacitors from different manufacturers, rated capacitance, and rated voltages. Instead, capacitors from 2 manufacturers were chosen that were of the same series, voltage, and capacitance ratings. For each manufacturer, three capacitor part numbers are chosen which presumably have no differences other than the package geometry. This statement is dependent on the assumption that capacitors of the same series from the same manufacturer with identical

electrical parameters only differ by geometry. Choosing capacitors from the same series and ratings, but different package geometries, we can minimize the variations in chemistry between capacitor part numbers and attribute differences in humidity-driven degradation to difference in package geometry only. All of the capacitors chosen for this test are 6.3V 470µF parts, and as in the preliminary HAST, test a sample size of 20 capacitors plus on control sample was used. In this Geometry-Based HAST test, only through-hole components are chosen. Additionally, dry heat testing was performed concurrently to compare the amount of degradation seen in dry versus humid conditions.

Table 3. Part Selection for Geometry-Based HAST Test

	Can Size 1 (mm x mm) (DxL)	Can Size 2 (mm x mm) (DxL)	Can Size 3 (mm x mm) (DxL)
Mfg. 1	6.3 x8.8	8.0x8.9	8.0x11.9
Mfg. 2	6.3x8.7	8.0x8.8	8.0x11.75

Table 4. Part Selection for Dry Heat Testing

	Can Size 1 (mm x mm) (DxL)	Can Size 2 (mm x mm) (DxL)	Can Size 3 (mm x mm) (DxL)
Mfg. 1	6.3 x8.8	8.0x8.9	8x11.9
Mfg. 2	6.3x8.7	8.0x8.8	8.0x11.75

2.2.3 Monitored Parameters & Measurement Equipment

Various electrical parameters were monitored during the HAST and dry heat testing. Capacitance, equivalent series resistance, and dissipation factor were monitored with an Agilent 4263B LCR meter using an Agilent 16047E test fixture (Figure 10), leakage current was monitored with an Agilent 4155C semiconductor parameter analyzer (Figure 11) using an Agilent 16442A test fixture, and weight was monitored with a Mettler AE 100 Analytical Balance (**Figure *12***). AC measurements of capacitance and dissipation factor were taken with a 120 Hz 1 VAC signal, and equivalent series resistance measurements were taken with a 100 kHz 1 VAC signal. Leakage current measurements were taken by applying the rated DC voltage of the capacitors for 120 seconds, at which time the current was measured. All measurements were taken at room temperature, and all capacitors were allowed time to cool to room temperature after being removed from the HAST and dry heat environments.

Figure 10. Agilent 4263B LCR Meter with surface-mount polymer aluminum capacitor

Figure 11. 4155C Semiconductor Parameter Analyzer (from Keysight.com)

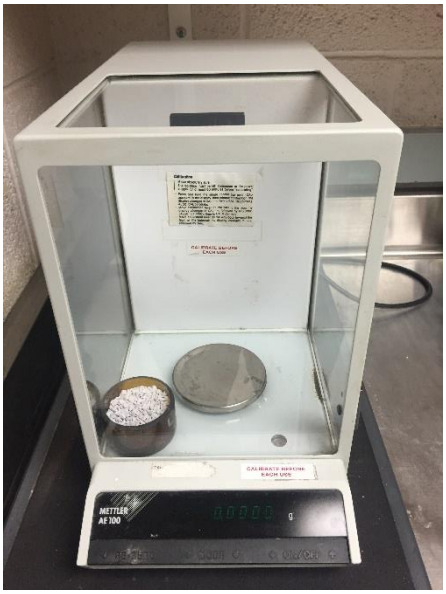

Figure 12. Mettler AE100 Analytical Balance

2.3 HAST Testing of Polymer Aluminum Electrolytic Capacitors

The testing sequence for both the HAST and dry oven testing can be seen in **Error! Reference source not found.**. Initial baseline electrical characterization was done on all capacitors upon being received (test time of 0 hours). Once capacitors had all their electrical parameters and weights measured, they were put into either the HAST Chamber or dry-heat oven, depending on their test conditions. After 50 or 100 hours of exposure, the chamber and oven were ramped down to room temperature, at which time the capacitors were removed and their weights and electrical parameters were measured. The parts were then placed back into the chambers which were ramped up to the HAST or dry heat conditions previously specified. Measurements were done a total of 12 times at the times shown on **Table *5***. At the conclusion of the testing, capacitors had been exposed to a total of 700 hours of HAST or dry heat exposure.

Table 5. Times at which measurements were taken

Measurement Times (hours)											
0	100	150	200	250	300	350	400	450	500	600	700

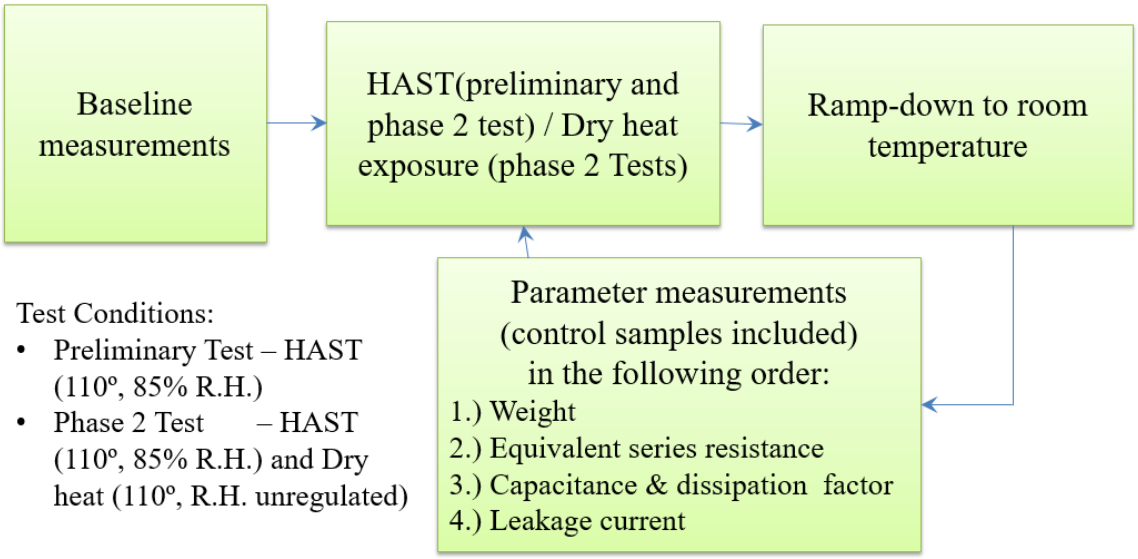

Figure 13. Testing sequence flowchart

2.3.1 Results of Preliminary HAST Test

The results of the Preliminary HAST testing showed that exposure to HAST conditions resulted in decreases in capacitance, and increases in equivalent series resistance, dissipation factor, leakage current, and weight for all capacitors. Results for the Preliminary HAST test of capacitors from different manufacturers and ratings are shown in the Appendix A. Furthermore, large differences in degradation were seen between different capacitor samples. An example of leakage current results from appendix A is shown below in Figure 14. This figure exemplifies the differences between capacitor samples of differing part numbers and manufacturers. For example, Figure 14 shows two capacitor samples, G and E, showing a large increase in leakage current at around 100 hours of testing. Alternatively, capacitor samples A and D do not show any increases in leakage current until the 400th hour of testing. Generally, surface mount capacitors experienced more degradation than through-hole capacitors. When comparing moisture uptake results between through-hole and surface mount capacitors, the results are

surprising. Although surface-mount capacitors experience higher rates of degradation, they experience lower rates of weight gain, or moisture absorption. On average, surface mount capacitors experienced a weight increase of 0.0038 grams at the end of the 700 hours of testing, while through-hole capacitors experienced on average a weight increase of 0.0098 grams. In terms of normalized percent weight gain, surface mount capacitors experienced on average a 0.93% weight increase, while surface mount capacitors experienced a 1.80% weight increase.

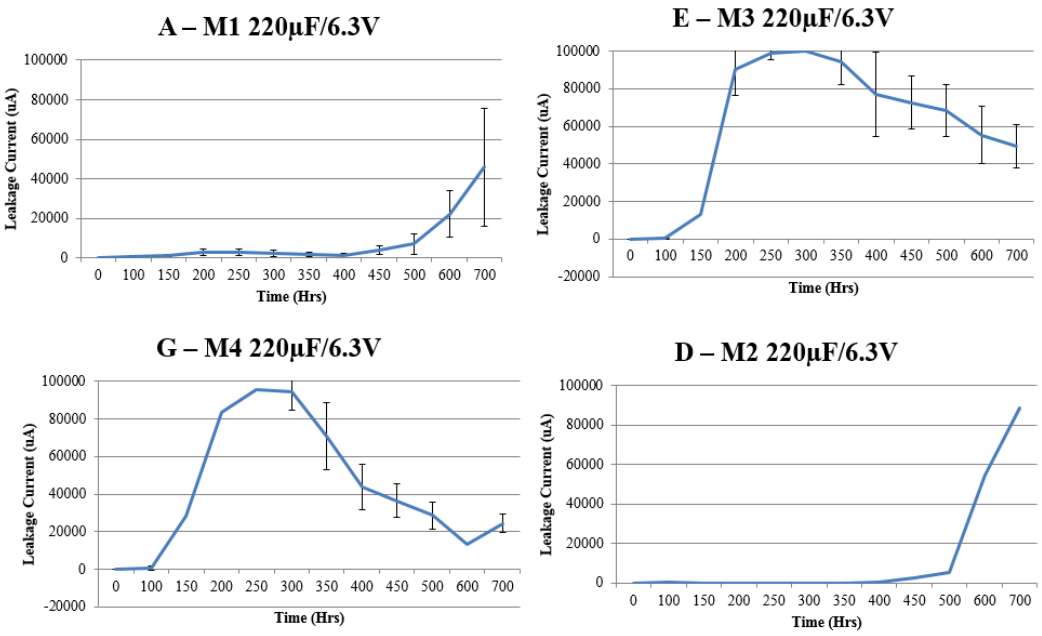

Figure 14. Example of leakage current results. Error bars represent 1 standard deviation.

2.3.2 Results of Geometry-Based HAST Test

The results for the Geometry-Based HAST test show changes in degradation rates between capacitor samples as seen in the Preliminary HAST tests. Capacitors from the same manufacturers that were of the same series and electrical ratings showed differences in degradation rates, suggesting that differences in capacitor degradation between samples can in part be due to differences in package geometry. The results of all of the electrical

parameter measurements from the Geometry-Based HAST tests can be found in Appendix B. An example of the differences in degradation seen between parts from the same manufacturer, electrical ratings, and same capacitor series are seen in **Figure *16***. Furthermore, it can be seen that the rates of moisture uptake for these capacitors are also slightly different, depending on the capacitor sample. As seen on the results plots on Appendix B, and the results on **Figure *17***, capacitors D and E (both from manufacturer 2) both show considerably higher degradation rates than the rest of the capacitors tested in the Geometry-Based HAST tests. As seen in **Figure *15***, those two capacitors also experienced the highest % weight increase throughout testing.

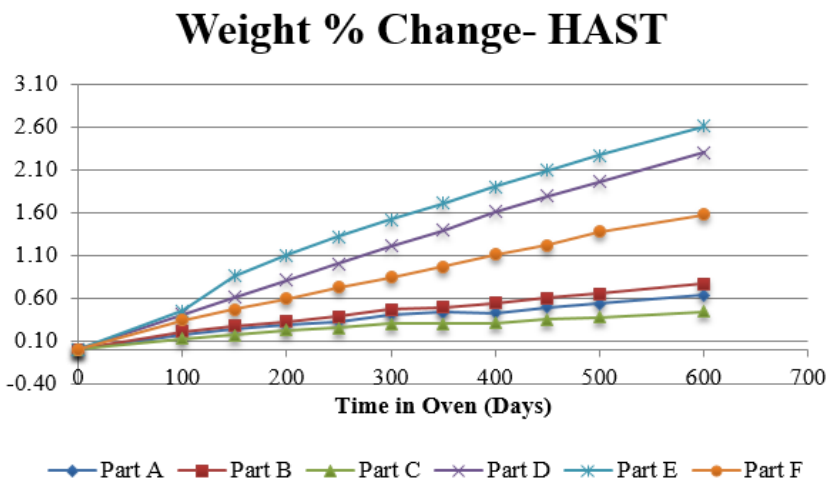

Figure 15. Percent weight change for capacitors in Geometry-Based HAST test

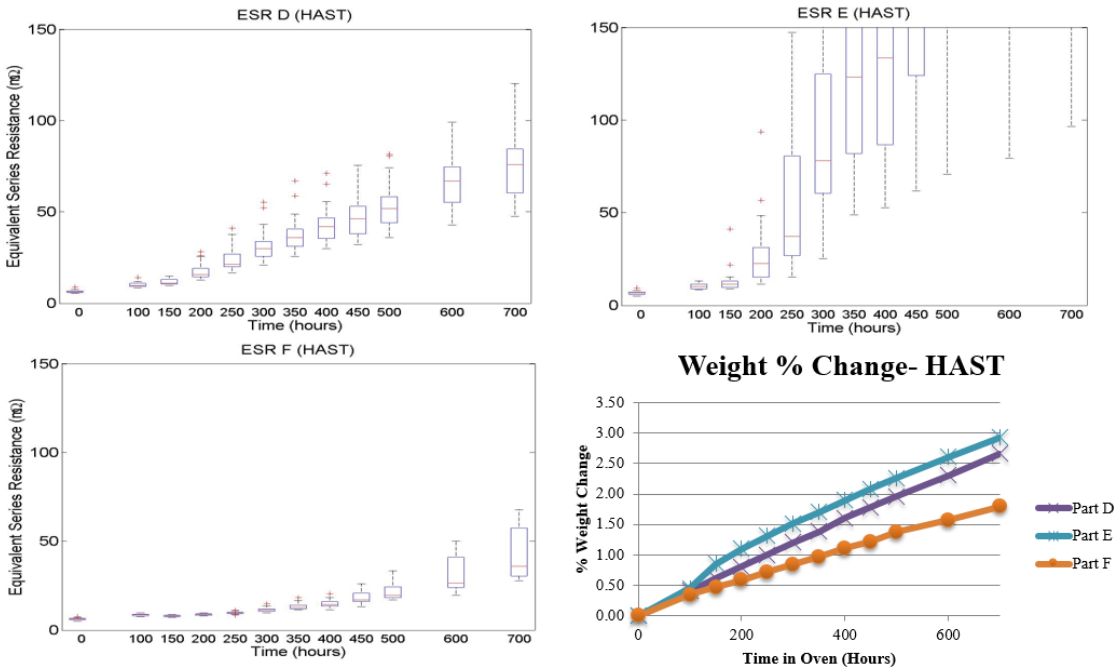

Figure 16. Equivalent Series Resistance Results for Capacitors of the Same Series and Electrical Ratings

2.3.3 Results of Dry Heat Testing

Dry heat testing (110°C, relative humidity unregulated) yielded almost no degradation in comparison to the degradation seen with HAST testing. Comparative result plots showing sample means for ESR and leakage current for the capacitors subjected to dry heat testing can be seen in **Figure *17***. Small changes in capacitance, leakage current, and ESR were seen in the first 100 hours of testing, but appeared to stabilize thereafter.

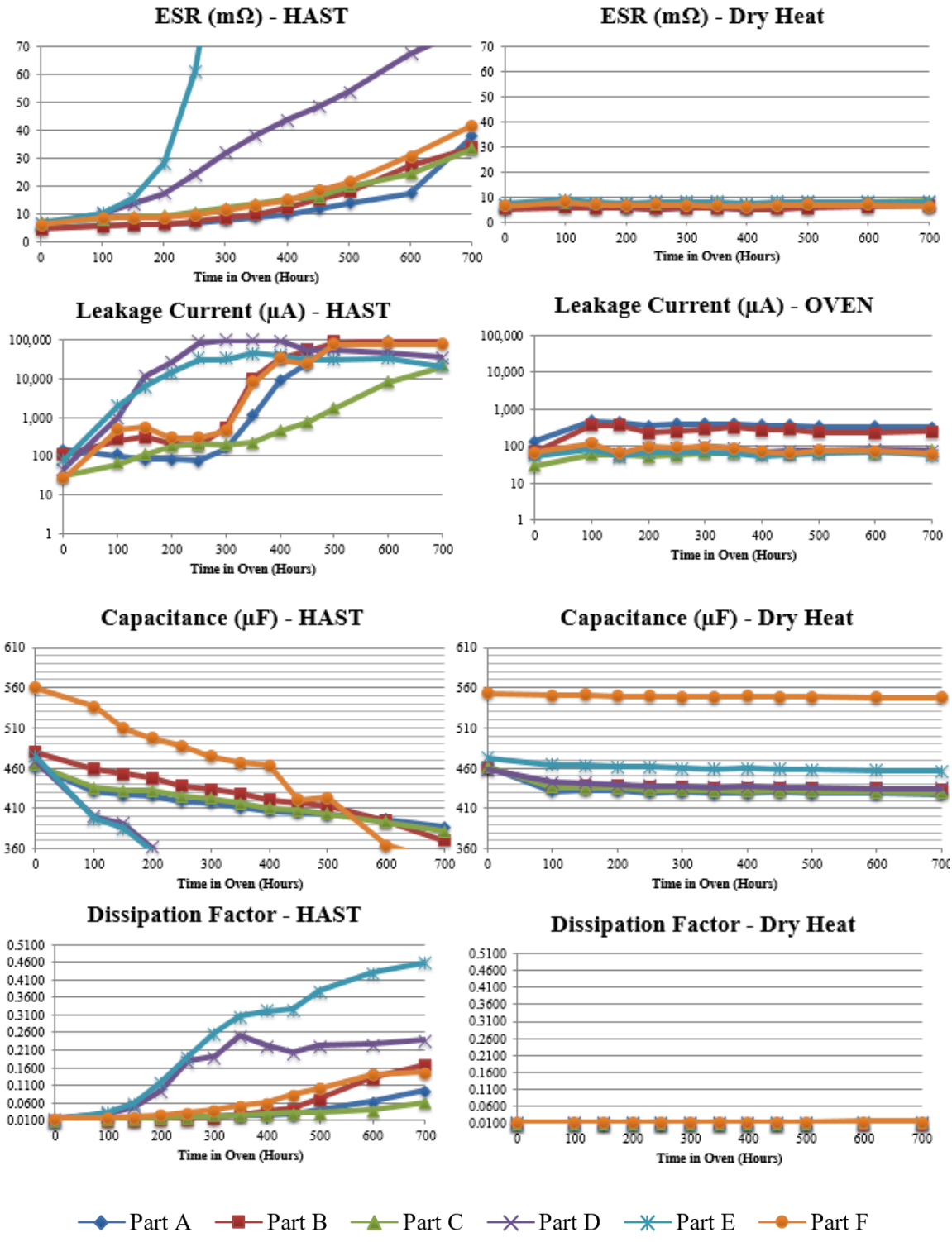

Figure 17. Results for HAST vs. Dry Heat testing

Chapter 3: Failure Modes and Mechanisms

3.1 Failure Modes

Failure criterion for the capacitors being tested were established to offer a basis for comparison between different capacitors. In this study, any of the following conditions were considered to represent a failure event: a capacitance reading that was 20% more or less than the rated capacitance; a 50% increase in ESR from the original values measured at time 0; a dissipation factor reading greater than 0.12; or leakage current readings greater than a value calculated by:

$$L.C. < 0.2 * (C*V).$$

While manufacturer failure criteria may differ slightly from the ones outlined in this paper, the criteria specified in this study were used to account for differences in failure criteria between manufacturers and provide an equal basis for comparison between capacitors. Parts exceeding the failure thresholds previously described were considered to have failed. For all of the HAST tests, the main failure modes at time of first failure were equivalent series resistance and leakage current. Table 6 shows the percentage of capacitors that failed by capacitance, dissipation factor, E.S.R., and leakage current at time of first failure. Some capacitors experienced more than one failure mode at time of first failure.

Table 6. Failure Modes at Time of First Failure

	Capacitance	Dissipation Factor	E.S.R.	Leakage Current
Preliminary HAST Surface-Mount	8.1%	6.9%	37.5%	76.9%
Preliminary HAST Through-Hole	2.5%	5.6%	79.4%	41.8%
HAST Test	4.1%	0.0%	56.70%	62.5%

3.2 Weibull Statistical Analysis

In order to provide a means for comparison between capacitor part numbers, the failure times of capacitors in a capacitor part number sample (20 capacitors per sample) were used to compute Weibull failure distribution parameters. A 2-parameter Weibull distribution is used to model the failure data of the sample parts. The Weibull distribution is used in accelerated tests and has been used to describe the life of roller bearings, electronics, and capacitors, among other things [25]. The 2-parameter Weibull cumulative distribution for population fraction failing is:

$$F(t) = 1 - e^{\left(-\left(\frac{t}{\eta}\right)^{\beta}\right)}$$

The two-parameters in a Weibull distribution are the shape parameter β and the scale parameter η (eta). The scale parameter η is known as the characteristic life, and represents the time at which the probability of failure is 63.2%. The scale parameter η has the same unit as the time (t) being used in the Weibull distribution equation. The shape parameter β can be seen as a measure of the spread of failure times. If β is greater than 1, a high β value indicates that parts are failing at times close to each other while a low β value indicates that part failures are more spread out. A β value greater than 1 indicates a wear out type of

failure mechanism, or increasing hazard rate over time. A β value of less than 1 means that the hazard rate, or instantaneous failure rate, decreases over time. This would be the case for a part experiencing infant mortality. A β value of 1 indicates a population with a constant hazard rate. In this report, the eta values of the capacitors proved the most useful in finding a relationship between failure times and capacitor geometric parameters.

3.3 Effect of Capacitor Geometry on Reliability

The Preliminary HAST test included capacitor samples of different rated voltages, capacitance, manufacturers, and series. However, even with a part selection process capable of introducing a large number of unknown factors between capacitor samples, a trend is seen when Weibull eta values are plotted versus a shape parameter referred to as the capacitor aspect ratio.

The aspect ratio of the capacitor is a parameter calculated from the geometry of the capacitor element inside the aluminum can. The capacitor element is comprised of the wound structure that includes the polymer PEDOT, paper separator, cathode and anode aluminum electrodes, and lead tabs. The aspect ratio of the polymer capacitors is calculated by dividing the length of the capacitor element (L_e) by the capacitor element diameter (D_e). The length and diameter of the capacitor element are illustrated in **Figure *18***. It should be noted that the aspect ratio is not a ratio of the length of the whole capacitor structure over the diameter of the capacitor structure, but is based on measurements of the capacitor element winding instead.

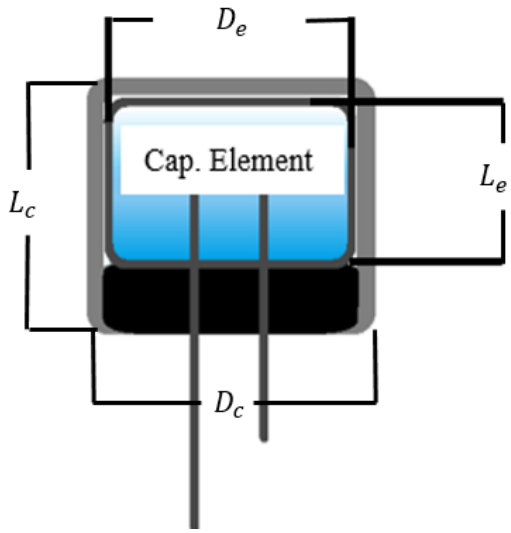

Figure 18. Representation of capacitor element dimensions

A trend of increasing Weibull eta parameters with increasing aspect ratio emerges when plotting eta values versus aspect ratio for the Preliminary HAST test. This trend can be seen in **Figure *19***. It is noteworthy that the surface mount capacitors all have an aspect ratio that is less than ~0.62, while through-hole capacitors all have an aspect ratio that is larger than ~0.62. Each point on **Figure *19*** represents the Weibull eta parameter calculated from the failure times of 20 capacitors.

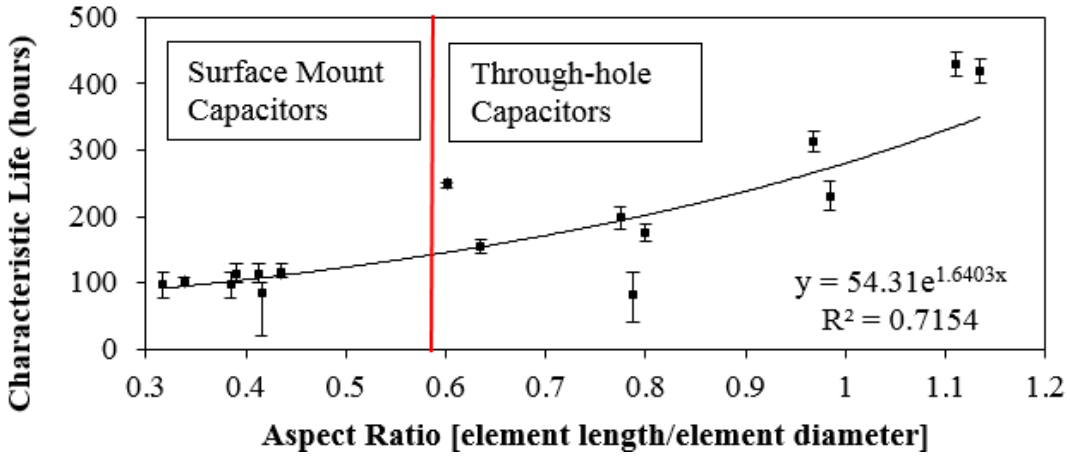

Figure 19. HAST Weibull Eta Values (Characteristic life) for Failures at Time of First Failure vs. Capacitor Aspect Ratio. Error bars represent Eta values with 90% confidence bounds.

The Geometry-Based HAST test, in which the part selection was aimed at limiting differences between capacitor samples to only geometry, showed slightly conflicting results. The aspect ratios of the capacitor elements and their eta values are seen in **Table 7**.

Table 7. Weibull eta values for Geometry-Based HAST test

Sample	Manufacturer	Aspect Ratio	Weibull Eta (hours)
A	M1	1.36	300
B	M1	1.17	247
C	M1	1.38	259
D	M2	1.27	46
E	M2	1.14	40
F	M2	1.27	183

In this case, the capacitors with the lowest aspect ratios from manufacturers 1 and 2 both have the lowest times to failures as expected from the trend seen in the Preliminary HAST test results, but sample A with an aspect ratio of 1.36 had a slightly higher eta value than capacitor C from the same manufacturer with a similar aspect ratio of 1.38. Capacitor D from manufacturer 2, which has an identical aspect ratio to capacitor F from manufacturer 2, had a much lower Weibull eta value of 46 hours compared to 183 hours for capacitor F. Additional analysis is required to understand these large differences in eta values although the capacitors have identical aspect ratios.

3.4 Failure Mechanisms

The following analysis techniques were employed to gain a better understanding of the failure mechanisms responsible for the degradation of these polymer aluminum capacitors in high temperature and humidity conditions.

3.4.1 Deconstruction of Polymer Aluminum Capacitors

To understand the differences between capacitors from manufacturers 1 and 2 from the Geometry-Based HAST test, the capacitors were analyzed destructively in thorough detail. One capacitor from each of the 6 capacitor samples from the Geometry-Based HAST test were chosen for this analysis. The purpose of this destructive analysis was to determine the amount of aluminum foil used in each capacitor, learn about differences in capacitor design between manufacturers, and to determine the relative weights of the aluminum and polymer used in the capacitors from both manufacturers. In order to separate the polymer from the aluminum foil in the capacitor element, the element was first removed from the aluminum can and the rubber bung. The capacitor elements were then placed in an oven at 500°C for 4 hours to de-compose the polymer. After the high temperature exposure, the capacitor elements were dipped in a dilute nitric acid solution to dissolve the most of the remaining polymer from the aluminum foil. The weight of the element winding was monitored prior to and after this process. The remaining material was the aluminum anode and cathode foils, with most of the polymer being removed as seen in **Figure *20*** and **Figure *21***.

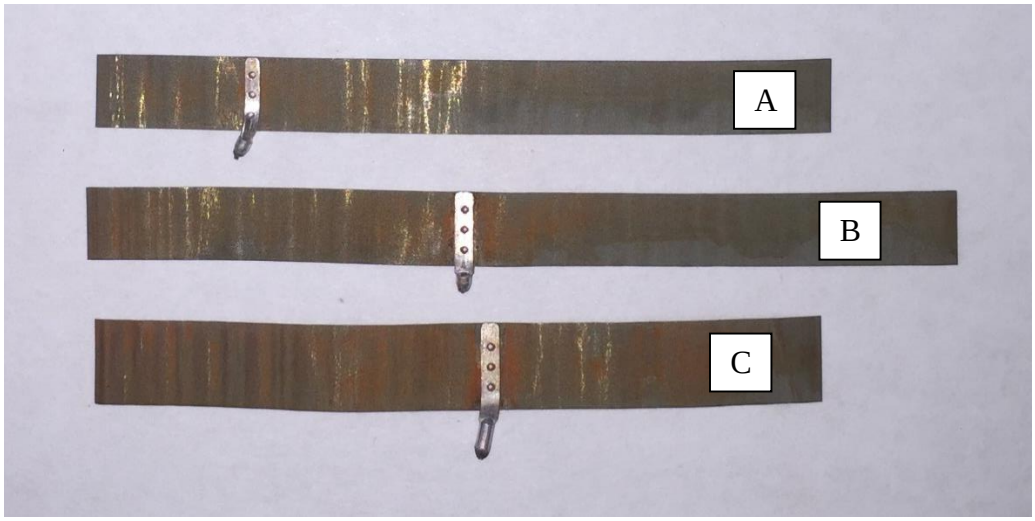

Figure 20. Anode foils from Geometry-Based HAST test capacitors (Mfg. 1)

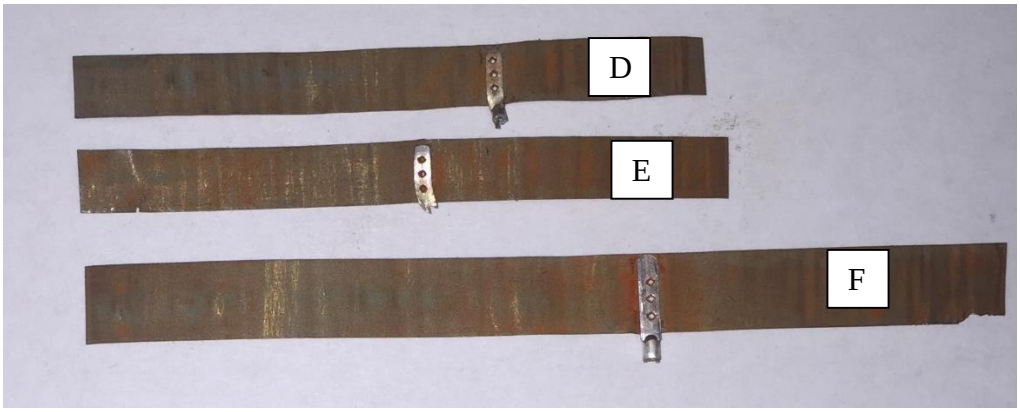

Figure 21. Anode Foils from Geometry-Based HAST test capacitors (Mfg. 2)

By monitoring the weight prior to the deconstruction process and after the bake-out and nitric acid dipping, the percent weights of the capacitors composed of the polymer PEDOT were calculated for each capacitor sample from the Geometry-Based HAST test. The percentage weights of PEDOT calculated from the process can be seen in **Table *8*.**

Table 8. Calculated % weight PEDOT

Sample	PEDOT (g.)	% Weight PEDOT
A	0.0573	~12.4
B	0.0719	~12.1
C	0.0834	~11.5
D	0.0714	~15.7
E	0.0722	~12.3
F	0.1444	~17.7

While samples A, B, and C from manufacturer 1 all contain similar percent weights of PEDOT, capacitor samples D and F from manufacturer 2 have higher amount of PEDOT, at 15.7-17.7%. Capacitor E has amounts of PEDOT similar to capacitors from manufacturer 1 at around ~12% PEDOT by weight, however, the times to failure for capacitor E (eta = 40 hrs.) were much lower than any capacitors from manufacturer 1 (eta = 247-300 hours). With the percent weight of the capacitors composed of PEDOT now calculated, the amount of moisture absorption in terms of the amount of PEDOT in the capacitors can be calculated. These values are shown on Table. 9.

Table 9. Average Percent weight PEDOT increase

Sample	Manufacturer	% Weight PEDOT Increase
A	Mfg. 1	6.8
B		8.3
C		5.5
D	Mfg. 2	19.3
E		25.9
F		10.8

It is difficult to make any conclusions from the % weight of PEDOT of the capacitors, since no clear correlations between the amount of PEDOT and degradation rates are seen. However, a correlation can be seen when the amount of moisture absorption in percent PEDOT weight increase is plotted versus the characteristic life of the capacitors.

This shows a correlation that is valid in capacitors between manufacturer 1 and manufacturer 2 capacitors, regardless of their seal quality. It can be seen that those capacitors that experienced the highest amounts of percent PEDOT weight increase saw the shortest times to failures.

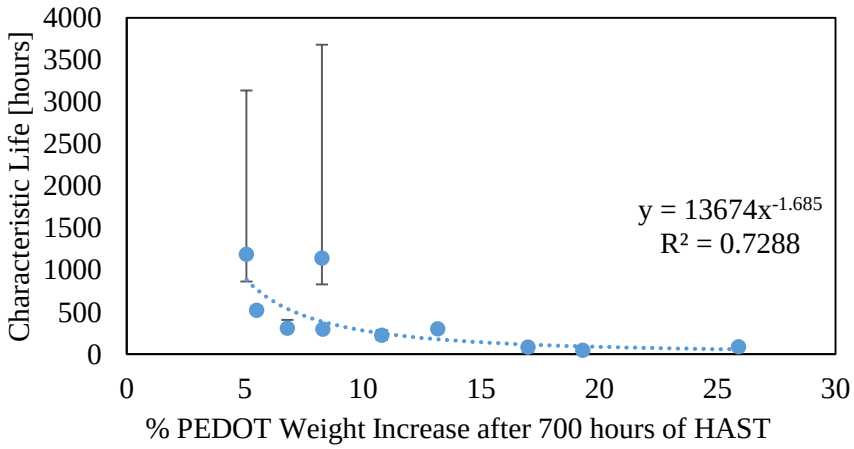

Figure 22. Characteristic life (Weibull eta) for leakage current failures versus the percent PEDOT weight increase after 700 hours of HAST

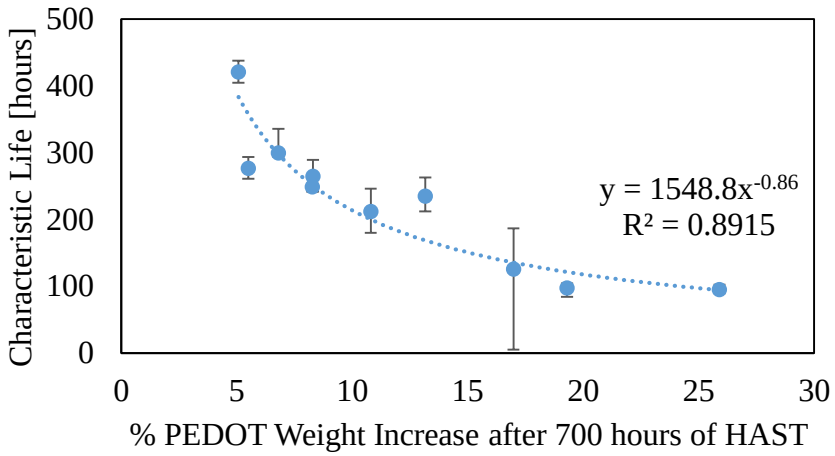

Figure 23. Characteristic life (Weibull eta) for ESR failures versus the percent PEDOT weight increase after 700 hours of HAST

The foils were then unrolled and their dimensions were measured in terms of length and height of the anode foil. The dimensional measurements can be seen in Table 10.

Table 10. Capacitor Foil Dimensions

Sample	Anode Length (mm)	Anode Height (mm)	Apparent Anode Surface Area (mm^2)
A	60	6	720
B	70	6	840
C	60	7	840
D	55	5	550
E	58	5	580
F	80	7	1120

The dimensions on Table 10 indicate design differences between manufacturers 1 (A- C) and manufacturer 2 (D – F). Manufacturer 1 uses the same anode foil length for capacitors A, and C, and uses a slightly longer length for capacitor B. Manufacturer 2 uses increasing foil lengths from capacitors D to F. Additionally, manufacturer 1 capacitor samples have similar anode surface areas (between 360 and 420 mm^2), while manufacturer 2 anode surface areas range from 275 mm^2 to 560mm^2.

The average capacitance values for each capacitor sample and the anode apparent surface area are used to calculate the capacitance (in µF) divided by the foil area (in mm^2) shown on Table 11. The capacitance per foil area is dependent on a number of factors, such as the dielectric constant of aluminum oxide dielectric layer, the thickness of the aluminum oxide dielectric layer, and the magnitude of etching of the aluminum foil during the manufacturing process. Instead of making assumptions to estimate the effective surface area of the capacitor and a multiple of the measured surface area of the foil, the capacity was listed in terms of capacity density per mm^2 of the unrolled anode foil.

Table 11. Capacity density by anode foil area

Sample	Capacitance (µF)/Al. Foil Area (mm^2)
A	0.60
B	0.57
C	0.55
D	0.79
E	0.81
F	0.50

The capacitance per area of aluminum foil shown in Table 11 shows that capacitors D and E, both which showed the highest amounts of degradation, have the highest concentration of capacitance per area of anode foil. These results would support the hypothesis that the same amount of diffusion of moisture into the capacitor element would affect capacitors with a higher concentration of capacitance more than capacitors with a lower concentration of capacitance. The low capacitance density on sample F also helps explain why capacitor F was closer in its degradation rates to the capacitors from manufacturer 1 although it had a higher rate of moisture absorption.

Finally, seal thicknesses were measured to determine whether seal thickness plays a role in the difference in moisture ingression between capacitors from manufacturer 1 and 2. The seal thicknesses can be seen in **Table *12***. Although the seal thicknesses in capacitors

from manufacturer 1 and 2 are similar, capacitors from manufacturer 2 experience around 3.5 times more weight increase than capacitors from manufacturer 1. Furthermore, the capacitor volumes and weights between manufacturers 1 and 2 do not show significant differences that would help account for the differences in weight gain between the two manufacturers. The difference in weight gain between manufacturers 1 and 2 can most likely be attributed to either rubber bung material differences, or seal quality, which includes the effectiveness of the crimping process of the aluminum can around the rubber bung.

Table 12. Geometry-Based HAST Test seal thicknesses

Sample	Seal Thickness	% Weight Increase at 700 Hours
A	1.8 mm	0.73
B	1.9 mm	0.85
C	2.9 mm	0.49
D	1.8 mm	2.67
E	2.3 mm	2.93
F	2.9 mm	1.79

3.4.2 Study of PEDOT Degradation by Raman Spectroscopy

Raman spectroscopy can be used to analyze PEDOT samples [26] [27] [28]. The Raman spectra of PEDOT have also been used to estimate doping levels of PEDOT samples. Raman spectroscopy relies on Raman scattering when illuminating a sample with a monochromatic light source such as a laser (between 244 nm and 1064 nm) [29]. Raman scattering, described by C.V. Raman in 1928, is a type of scattering characterized as an inelastic collision between an incident photon and a molecule where the vibrational energy of the molecule is altered, resulting in a small change in the energy between the excitation photon from the scattered photon [30].

A Raman microscope amplifies the wavelength shifts of the inelastic scattered light and gives results in the format of a Raman spectrum/spectrograph. The Raman spectrum of the polymer PEDOT shows several peaks that are described by different vibrational modes. A study by Chiu et al. shows how the Raman spectrum of PEDOT changes with differences in doping levels. **Figure *24*** shows the Raman spectrum of a neutral (de-doped) sample of PEDOT [27]. In the same study by Chiu et al., neutral PEDOT samples were electrochemically sulfate-doped at different doping levels, which was achieved by doping the polymer electrochemically at different potentials. The results for this can be seen in **Figure *25*.**

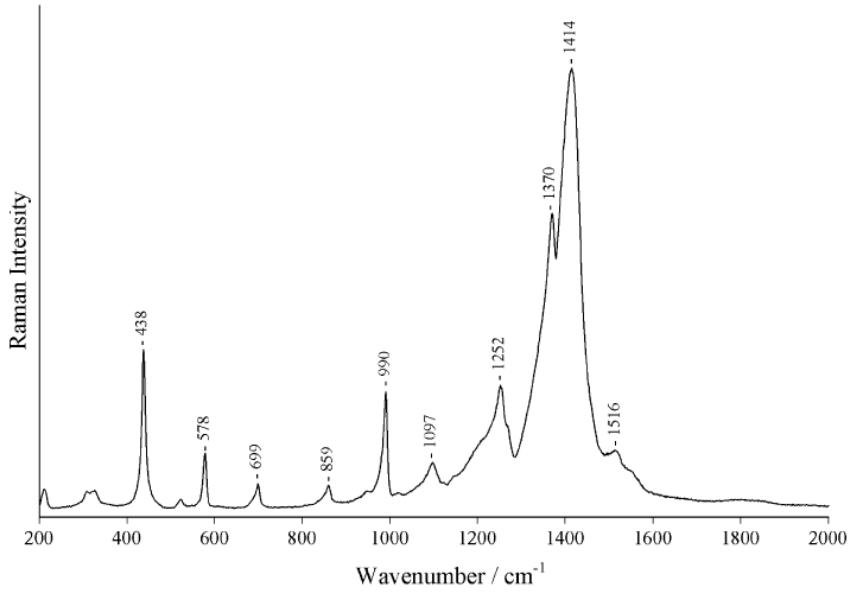

Figure 24. Raman spectra of neutral PEDOT with an excitation wavelength of 785 nm *[27]*

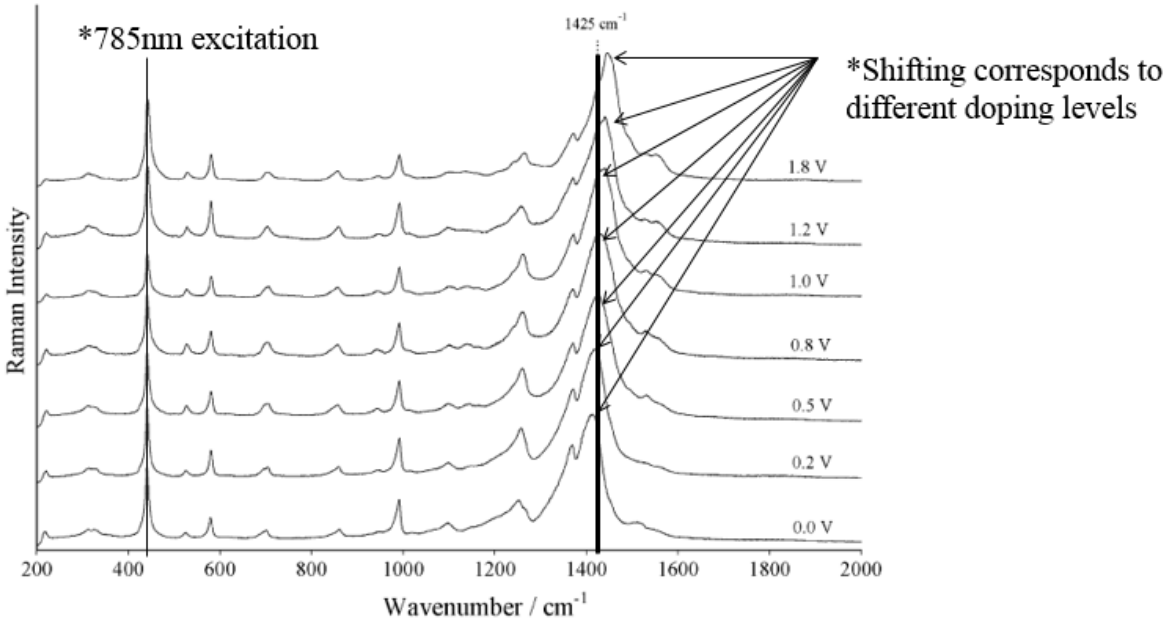

Figure 25. Raman spectra of PEDOT doped electrochemically at different potentials *[27]*

Chiu at al. were able to show that with increasing doping levels (higher doping levels yield more conductive PEDOT samples), there was shift in one of the PEDOT Raman spectra peaks centered around 1425 cm^{-1} as seen in **Figure *25***.

Since Raman spectroscopy can be used to draw conclusions regarding the doping levels of PEDOT, Raman spectroscopy of capacitors after exposure to HAST testing, and capacitors that had not been exposed to HAST conditions was done. The objective of Raman spectroscopy of the PEDOT in tested and new polymer aluminum capacitors was to determine if moisture in the capacitors affects PEDOT by leading to de-doping of the polymer, and thus determine one of the failure mechanisms of polymer aluminum capacitors in high-humidity conditions. Additionally, Raman spectra of the polymer were taken at different foil locations to determine the existence of any gradients in polymer doping levels after HAST testing, which could indicate gradients in moisture content within the element winding to help determine the path of diffusion of moisture into the capacitor element.

The equipment used for Raman spectroscopy of the polymer on polymer aluminum capacitors was a Yvon Jobin LabRam ARAMIS Raman microscope. An excitation wavelength of 633 nm was used for all the Raman spectra acquired during this study. The microscope settings used to acquire Raman spectra of PEDOT on the polymer capacitors can be found in Table 13.

Table 13. Raman microscope settings

Microscope Setting	Value
Filter	D1
Hole	400 μm
Slit	100 μm
Grating	600
Spectrometer Offset	1550 cm^{-1}
Exposure Time	10 seconds
Average	10 measurements per spectrum
Magnification	10x

The capacitor samples used for the study had been exposed to 700 hours of HAST testing at 110ºC and 85% relative humidity. Raman spectroscopy of capacitor samples was done 5 days after the last exposure to HAST conditions. Capacitors were stored at room temperature during the 5 days after HAST exposure and prior to Raman spectroscopy. The capacitors chosen for analysis using Raman spectroscopy were from manufacturer 2 from the Geometry-Based HAST tests. These capacitors experienced the most drastic degradation and shorter times to failure, as well as the highest amounts of moisture

absorption. Capacitor samples were prepared by first removing the capacitor elements from the aluminum can, and then unrolling the capacitor elements as seen in **Figure *26***. This was done immediately prior to the Raman spectroscopy analysis to minimize any moisture absorption that could occur from the ambient conditions. Once the capacitor elements were unrolled, they were placed in the Raman microscope and analyzed.

Figure 26. Unrolled capacitor element of polymer aluminum capacitor after HAST exposure

The unrolled capacitor elements were analyzed at the approximate location shown on Figure 27. The dark-colored coating on the aluminum foils seen in Figure 24. is the conducting polymer PEDOT.

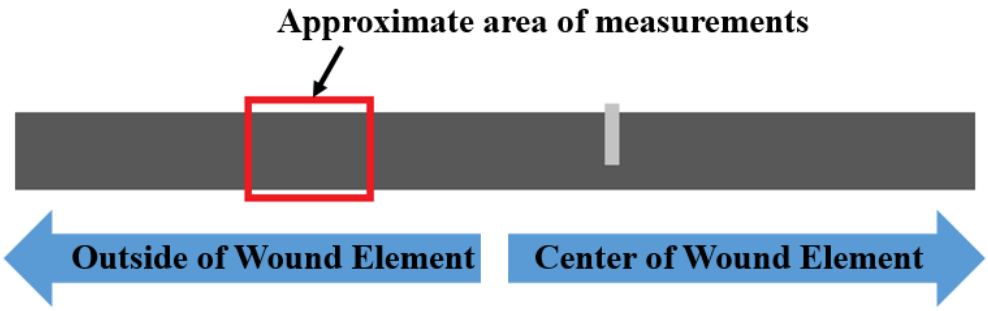

Figure 27. Approximate location of Raman measurements on unwound anode foil

Inside the approximate location of measurements shown on Figure 27, measurements were taken at locations 1, 2, and 3 shown on Figure 28 on both a new healthy capacitor that had not been exposed to HAST, and a failed capacitor (capacitor F from manufacturer 2) that had been exposed to 700 hours of HAST. Location 1

corresponds to the top of the capacitor element winding, 2 corresponds to the center of the capacitor winding, and 1 corresponds to the bottom of the capacitor winding.

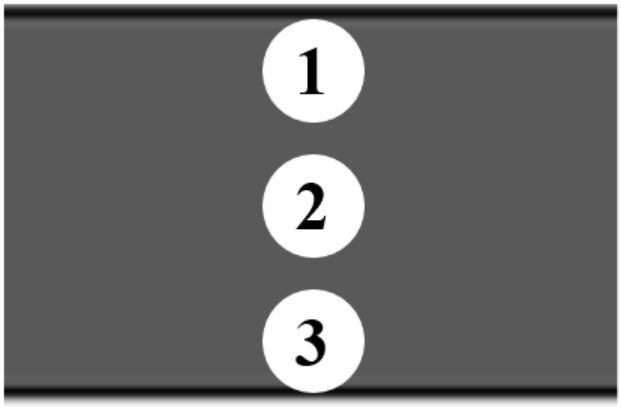

Figure 28. Representation of 3 approximate Raman measurements sites

A sample of Raman spectra taken at different locations of a failed capacitor is shown on Figure 29. It can be seen that along the top (location 1) and bottom (location 2) of the capacitor winding, the doping-related Raman peak is at around 1429 cm^{-1}, while the center of the capacitor element shows a peak at 1438 cm^{-1}. These results show that the polymer PEDOT is more de-doped along the top and bottom of the capacitor element than the center. The Raman spectrum of an untested and healthy capacitor is shown on the same figure, and the doping-associated peak is at 1444 cm^{-1}. A healthy capacitor measured at the same locations shown on Figure 28 did not show large differences in doping levels like the ones seen in the failed capacitor. Repeated measurements along the 1 (top), 2(center) and 3(bottom, closest to seal) locations of a new capacitor and failed capacitor are shown in **Error! Reference source not found.**.

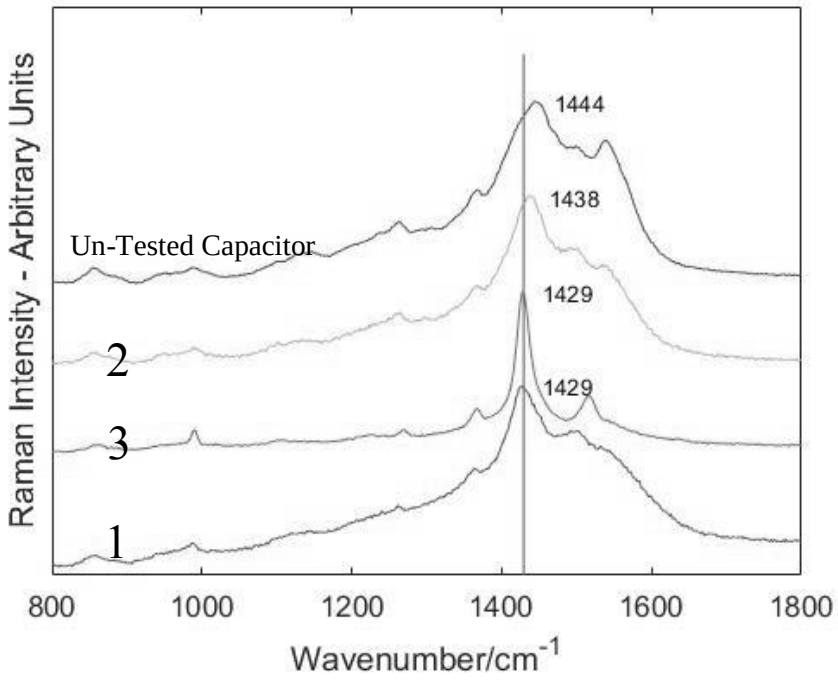

Figure 29. Raman spectra of PEDOT at different capacitor locations

While Fig. 28 shows example results from testing, repeated measurements were taken from 4 capacitors. A total of 5 measurements taken along the top, center, and bottom of the capacitor elements from a failed sample E manufacturer 2 capacitor, failed sample F manufacturer 2 capacitor, failed sample C manufacturer 1 capacitor, and healthy sample F manufacturer 2 capacitor. The results are for the peak values are shown as boxplots in the following figures. It can be seen that the trend of higher peak values at the center of the capacitor are seen in both manufacturer 1 and manufacturer 2 capacitors.

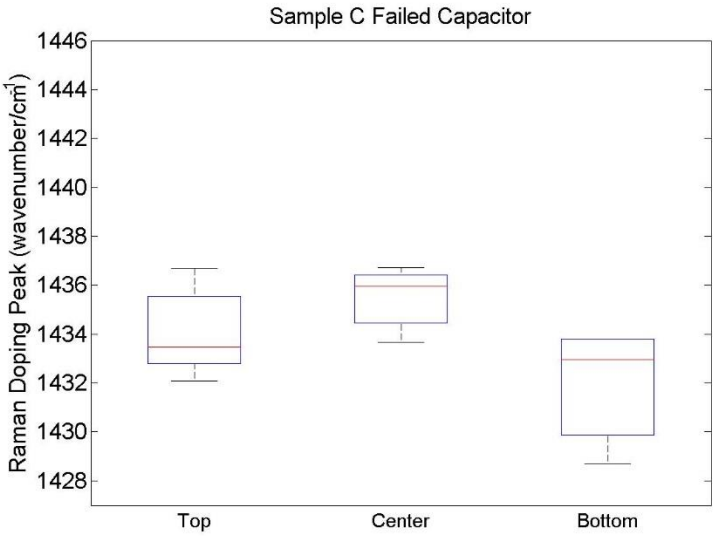

Figure 30. Raman peak values for sample C manufacturer 1 failed capacitor

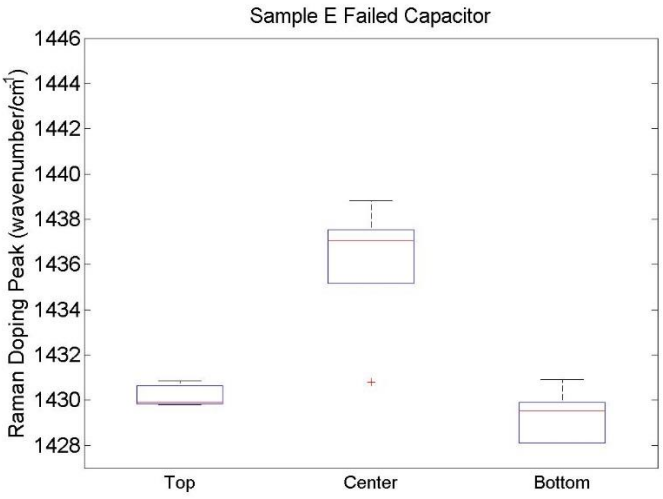

Figure 31. Raman peak values for sample E manufacturer 2 failed capacitor

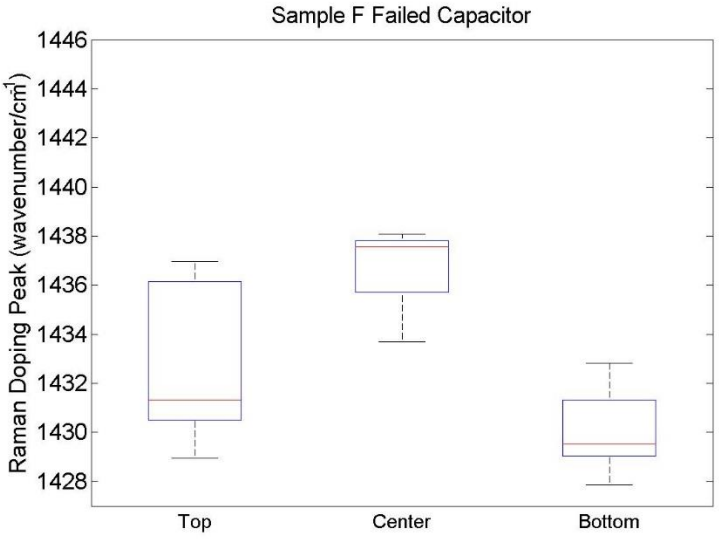

Figure 32. Raman peak values for sample F manufacturer 2 failed capacitor

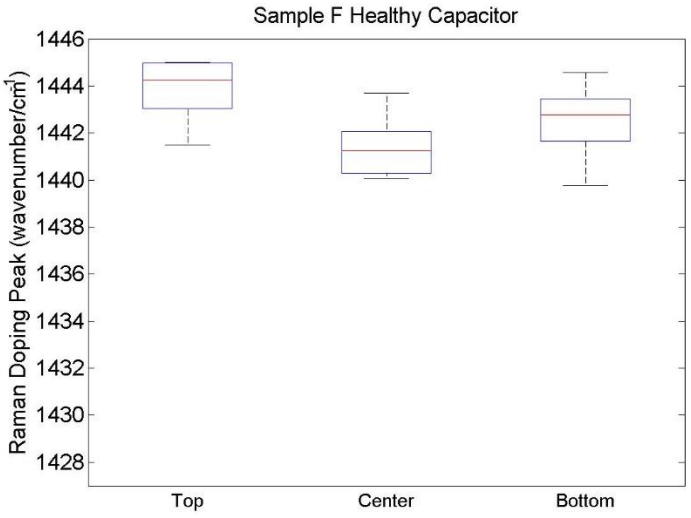

Figure 33. Raman peak values for sample F manufacturer 2 healthy capacitor

3.4.3 X-ray Imaging

X-ray images were taken of healthy, un-tested capacitors as well as failed capacitors from the Geometry-Based HAST tests at the conclusion of the 700 hours of exposure. X-ray images were taken using a GE Nanomex X-ray system. The purpose of the x-ray inspection of the new and tested capacitors was to see if any noticeable swelling of the capacitor was present as a result of weight gain through moisture absorption. While x-ray images of capacitors from manufacturer 1 from the Geometry-Based HAST tests did not show noticeable differences between tested and healthy capacitors, noticeable swelling was seen in capacitors from manufacturer 2 which experienced higher increases in weight due to moisture absorption (10 – 16% weight PEDOT increase). Assuming all of the weight increase in the capacitors is through the absorption of moisture by the polymer PEDOT, the percent weight increases of PEDOT at the end of the 700 hours of HAST exposure can be seen in **Error! Reference source not found.**. These values can be related to the amount of swelling in the polymer since thin films of PEDOT are known to swell by up to 50% in 82% relative humidity depending on the type of PEDOT [4].

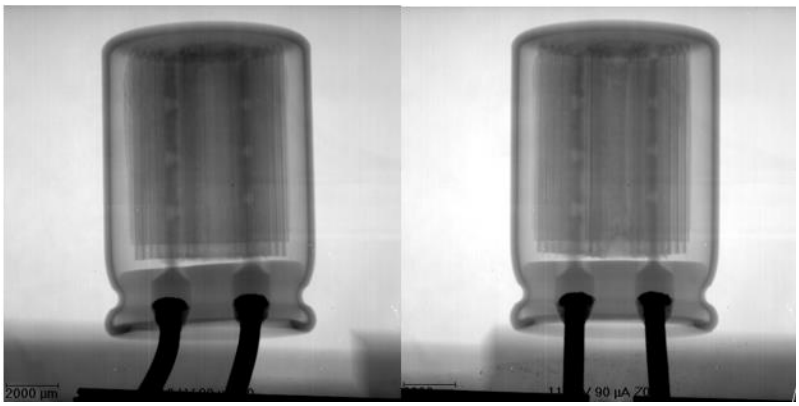

Figure 34. X-ray image of healthy capacitor (right) and failed capacitor (left) – A from Geometry-Based HAST test

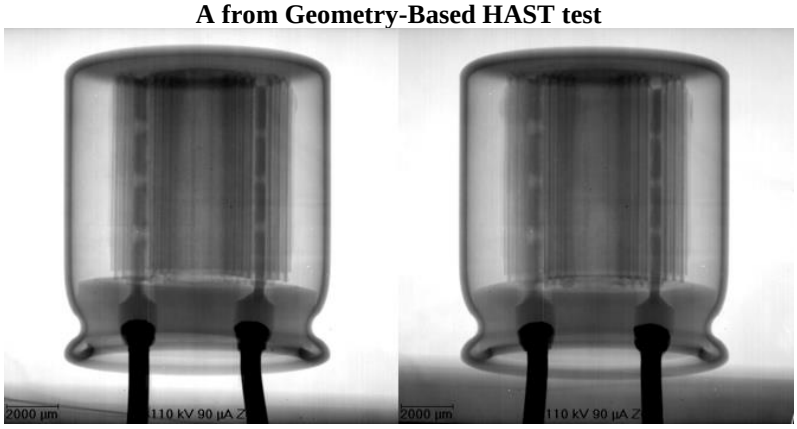

Figure 35. X-ray image of healthy capacitor (right) and failed capacitor (left) – B from Geometry-Based HAST test

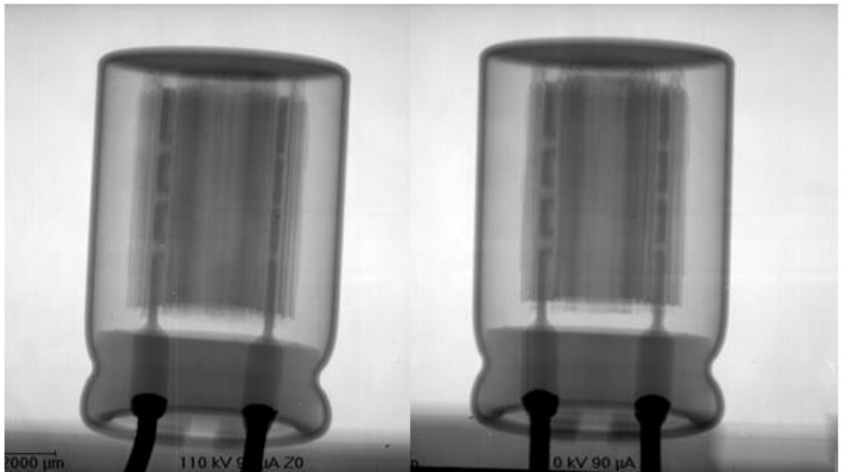

Figure 36. X-ray image of healthy capacitor (right) and failed capacitor (left) – C from Geometry-Based HAST test

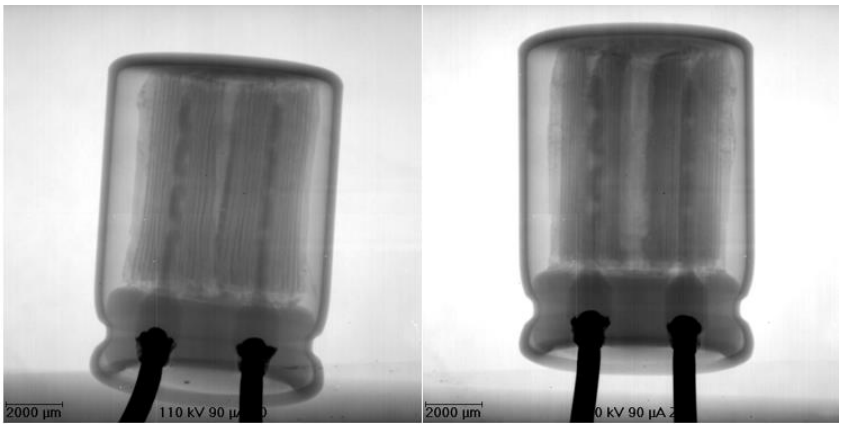

Figure 37. X-ray image of healthy capacitor (right) and failed capacitor (left) – D from Geometry-Based HAST test

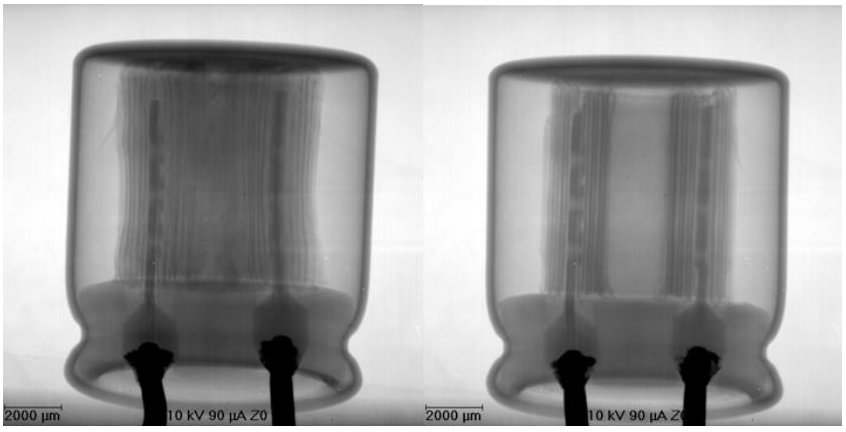

Figure 38. X-ray image of healthy capacitor (right) and failed capacitor (left) – E from Geometry-Based HAST test

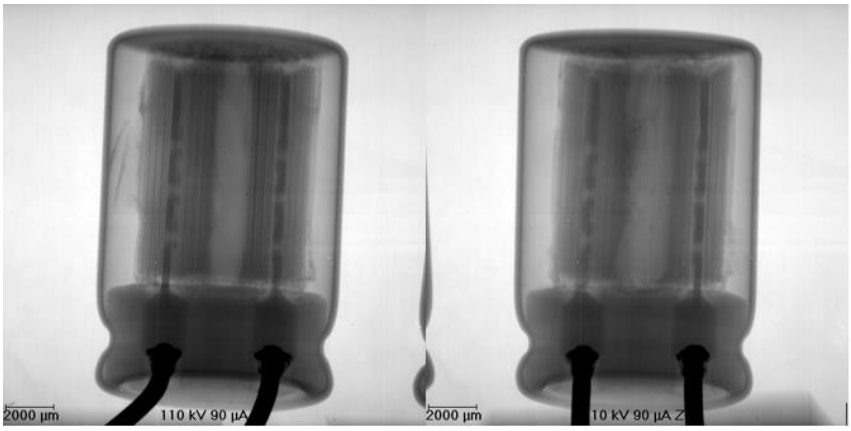

Figure 39. X-ray image of healthy capacitor (right) and failed capacitor (left)) – F from Geometry-Based HAST test

Capacitors D, E, and F seen in Figure 37-33 show swelling, especially near the top and the bottom of the capacitor elements. This is consistent with the hypothesis that the path of moisture diffusion into the capacitor element occurs axially. This is in agreement with the highest levels of de-doping seen through Raman spectroscopy near the top and bottom of the capacitor elements. As much as a 6-10% expansion in PEDOT layer thickness is estimated with the use of the x-ray images.

3.4.4 Environmental Scanning Electron Microscopy

Further analysis of the failed capacitors was done through environmental scanning electron microscopy (E-SEM). A state-of-the-art FEI Quanta Environmental Scanning Electron Microscope was used to acquire image of capacitor cross sections that were potted in epoxy, and grinded. Polishing of the sample with a polycrystalline alumina solution was not done to eliminate the possibility of particulates that could get lodged on the soft polymer. The capacitor samples chosen for E-SEM were from the Geometry-Based HAST tests. A capacitor from sample E of manufacturer 2 was cross sectioned because it was expected to show the most amount of degradation due its very low time to failure and large moisture absorption rate (Figure 41). A healthy capacitor was also cross-sectioned for scanning electron microscopy for comparison (Figure 42). From this extreme case of degradation, it is apparent from the figures that the swelling of the polymer PEDOT has caused significant deformation of the anode and cathode foil layers (Figures 35,37).

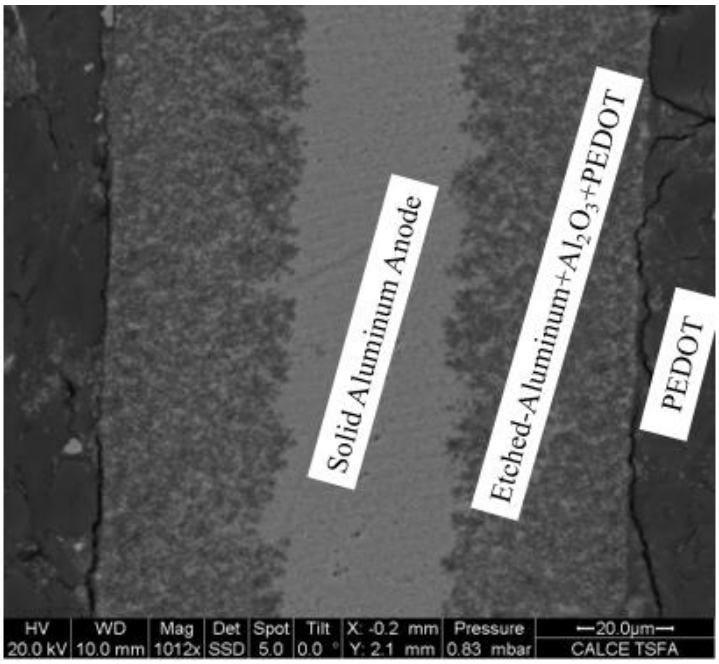

Figure 40. ESEM image of anode/dielectric/polymer interface cross section of a healthy capacitor

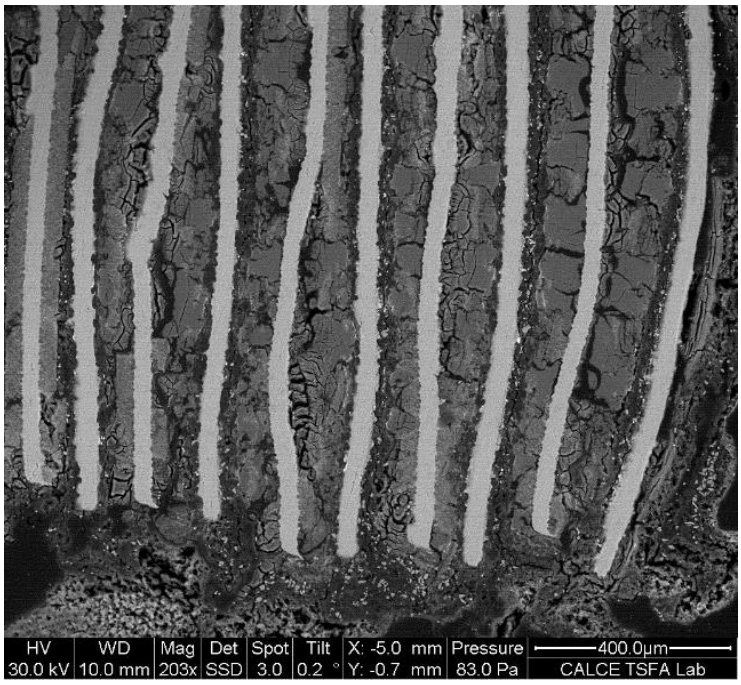

Figure 41. Scanning electron microscope image of failed capacitor element

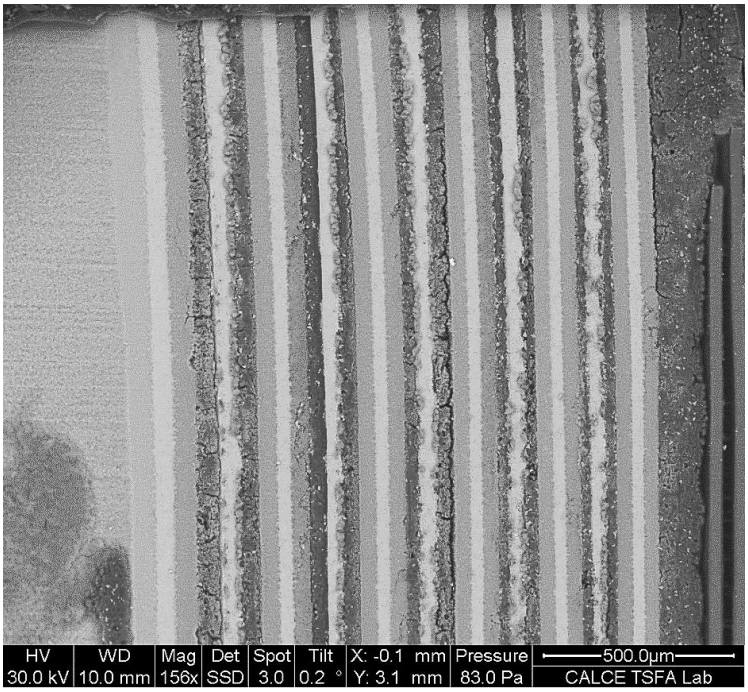

Figure 42. Scanning electron microscope image of healthy capacitor

The image in Figure 43 shows an area of the anode/etched-anode/dielectric interface which has been damaged through deformation likely caused by the expansion of PEDOT upon moisture absorption. An illustration explaining the process by which the expansion of PEDOT could result in the separation of the etched portion of the anode from the solid portion of the anode can be seen in

Figure ***44***. A combination of this mechanical deformation process, and the dissolution of the thin barrier oxide layer by the formation the acidic solutions described in the literature review section are likely the failure mechanisms leading to an increase in leakage current with the absorption of moisture. The leakage paths caused by possible dissolution of the aluminum oxide and mechanical damage as a result of PEDOT expansion can then lead to high-leakage paths accompanied by heat generation and melting of the aluminum/aluminum oxide/polymer region. This is possibly seen as a change in surface morphology of the damaged areas in Figure 37 from a rough anode/dielectric/polymer

interface area to a smooth area where localized heating may have melted the aluminum and fused the materials together to form a more homogeneous material.

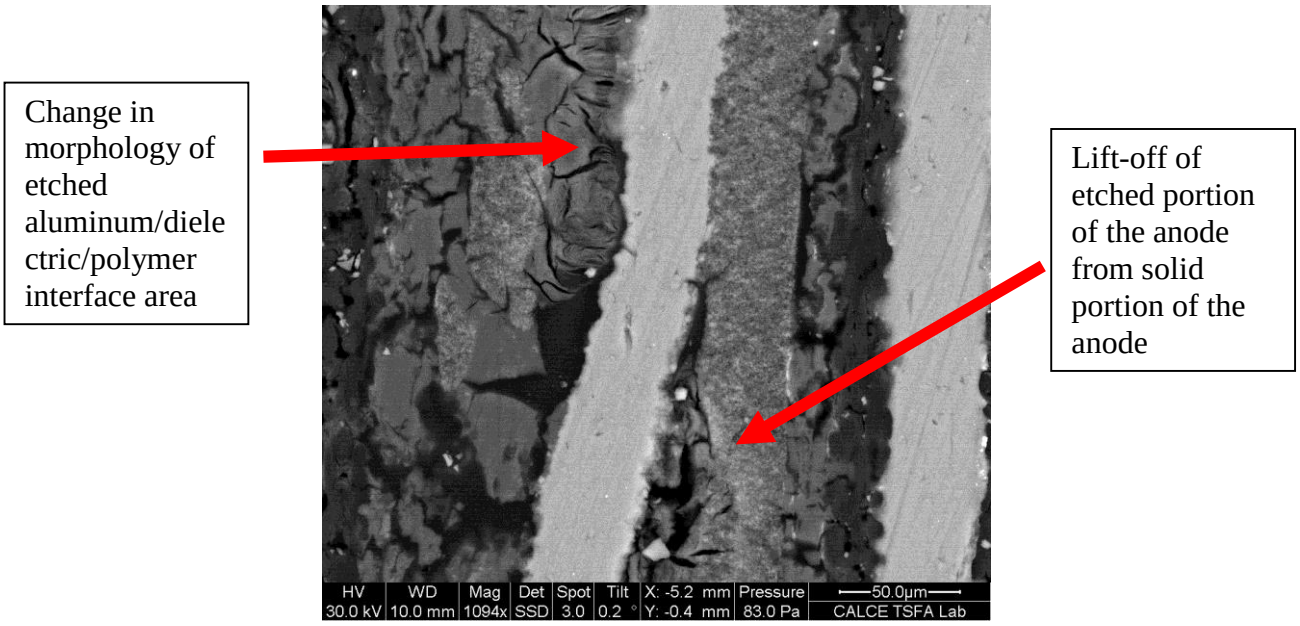

Figure 43. ESEM image of anode/dielectric/PEDOT interface with extensive damage

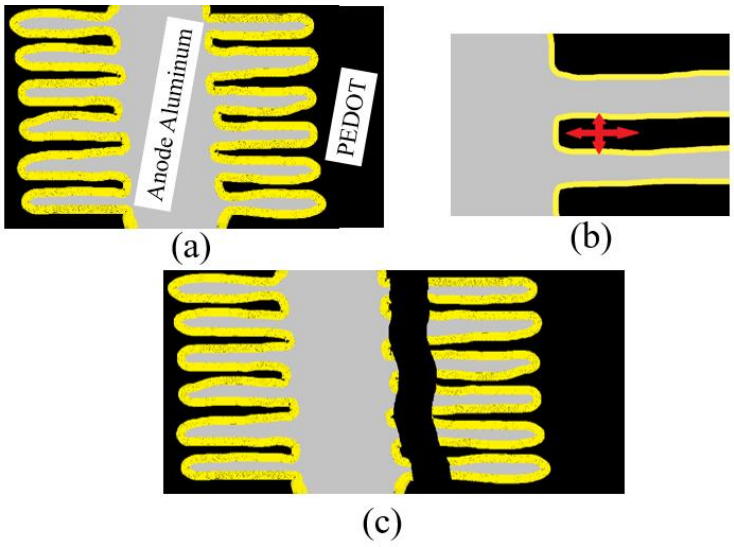

Figure 44. Illustration of possible mechanical damage to anode foil by expanding PEDOT

(a) simplified representation of etched anode (grey) with thin oxide (yellow) and PEDOT (black). (b)Isotropic expansion of PEDOT through moisture absorption projects stress onto etched portion of aluminum. (c) Stress from PEDOT expansion resulting in "lift off" of etched aluminum columns from solid anode

Chapter 4: Conclusions

HAST conditions at (110°C and 85% relative humidity) were used to precipitate moisture-driven failures in polymer aluminum capacitors. Results from HAST testing showed that surface mount capacitors failed earlier than through-hole capacitors, and the dominant failure modes precipitated during testing were high leakage current and high equivalent series resistance.

A correlation between capacitor geometry and times to failure was observed, suggesting that capacitors containing element windings with a lower aspect ratio were overall more susceptible to humidity-related degradation than capacitors with higher aspect ratios. An additional HAST test aimed at better understanding the effects of package geometry on humidity-related degradation showed that the capacitors with the lowest aspect ratios showed the smallest times to failure. These results also showed that out of two capacitors with the same length, but different diameters, the capacitor with larger diameter will experience a larger weight increase in terms of % weight increase than the capacitor with the smaller diameter, even if it has a slightly thicker seal. Furthermore, of two capacitors with identical diameters, but different lengths, the capacitor with the largest length experienced less weight increase in terms of percent weight increase, possibly due to that capacitor having a thicker seal.

The capacitors from the Geometry-Based HAST test were analyzed in detail to understand the failure mechanisms of polymer aluminum capacitors exposed to high temperature and humidity conditions. Raman spectroscopy was used to determine that the polymer PEDOT was degrading due to the absorption of moisture into the capacitor

winding element. Higher amounts of polymer degradation in terms of de-doping were seen along the top and bottom of the capacitor element winding, consistent with x-ray images of failed capacitors showing swelling near the top and bottom of the capacitor element winding. The discovery of the diffusion path of moisture into the capacitor element axially from the top and bottom of the winding partly explains the geometric relation seen between aspect ratio and times to failure. The diffusion path of moisture into the capacitor element winding is longer for a capacitor with a larger length.

Lastly, scanning electron microscopy was used to determine that the failure mode in increase in leakage current can at least in part be attributed to mechanical deformations and damage to the thin aluminum oxide dielectric by the expansion of the polymer PEDOT upon the absorption of moisture.

Chapter 5: Contributions

- Provided the first analysis of a relationship between capacitor geometric parameters and failure times in polymer aluminum capacitors exposed to high temperature and humidity.
    - Increase in capacitor diameter results in increased moisture uptake, while an increase in capacitor length increases the path for diffusion of moisture into the capacitor element winding, lowering the rate of degradation due to moisture absorption.
- Identification of a new failure mechanisms of polymer aluminum capacitors subjected to HAST (110ºC, 85% R/H.) conditions for the failure mode of high ESR.
    - The absorption of moisture by the polymer PEDOT results in the de-doping of the polymer, as was shown by Raman spectroscopy, leading to a decrease in polymer conductivity and increase in equivalent series resistance.
- Identification of a new failure mechanisms of polymer aluminum capacitors subjected to HAST (110ºC, 85% R/H.) conditions for the failure mode of high leakage current.
    - Increase in leakage current can in part be attributed to mechanical deformation at the anode/dielectric/PEDOT interface due to the expansion of PEDOT upon moisture absorption.

Chapter 6: Future Work

To evaluate the differences in sealing quality between capacitor manufacturers like the ones seen between manufacturers 1 and 2 from the Geometry-Based HAST Test, the rubber bung material should be characterized. It is possible that differences in seal material selection between capacitor manufacturers was the cause for the large differences in moisture uptake between two capacitor manufacturers.

Additional HAST testing of polymer aluminum capacitors should be done where capacitors at different stages of degradation are cross sectioned and studied using transmission electron microscopy (TEM). TEM would make it possible to magnify polymer aluminum capacitor cross sections to a magnification high enough to see the degradation of the dielectric layer in detail. This type of microscopy work would make it possible to determine whether mechanical stresses from PEDOT expansion or dielectric layer dissolution from the formation of acid solutions is the dominant failure mechanism resulting high leakage current. This level of magnification would also make it possible to quantify differences in etching density of the aluminum anode, and would allow for direct measurements of the dielectric thickness.

Finally, the work in this thesis focused on the more traditional cylindrical-type (wound) polymer aluminum electrolytic capacitors, but did not study the newer alternative configuration which is a plastic-encapsulated rectangular polymer aluminum capacitor. The susceptibility of these capacitors to high humidity conditions should be studied, since geometry has been shown to play a role on the path of moisture diffusion and reliability in high humidity conditions.

Appendices

Appendix A – Results from Preliminary HAST Testing

1. Capacitance Results

Capacitance – SMT 220µF

A – M1 220µF/6.3V

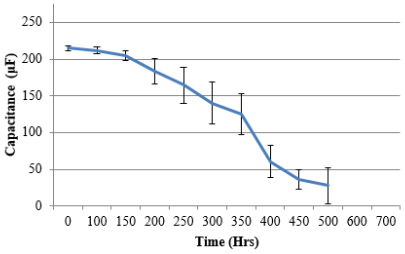

D – M2 220µF/6.3V

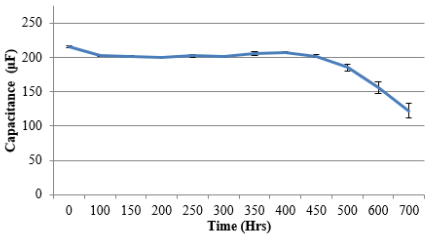

E – M3 220µF/6.3V

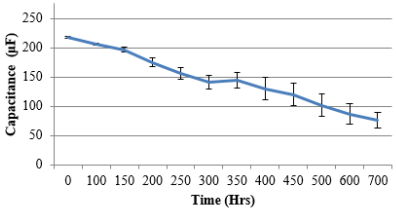

G – M4 220µF/6.3V

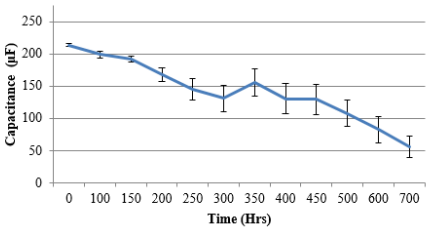

Capacitance – SMT 330µF

B – M1 330µF/2.5V

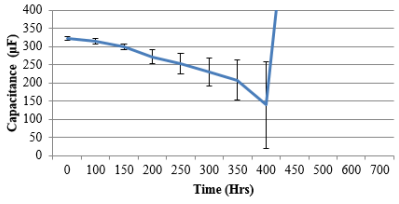

C – M2 330µF/2.5V

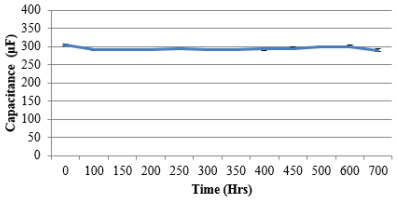

F – M3 330µF/2.5V

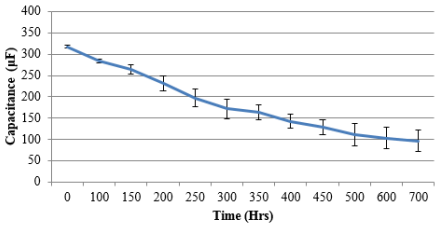

H –M4 330µF/2.5V

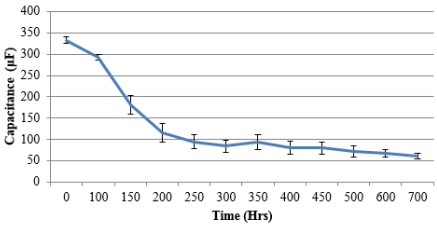

Capacitance – TH 560µF

I – M5 560µF/6.3V

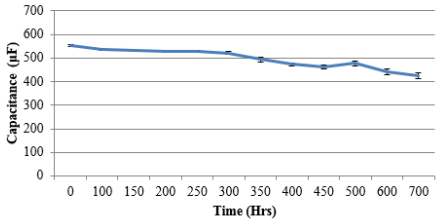

J – M5 560µF/6.3V

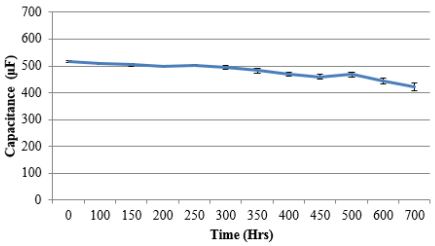

L – M5 560µF/6.3V

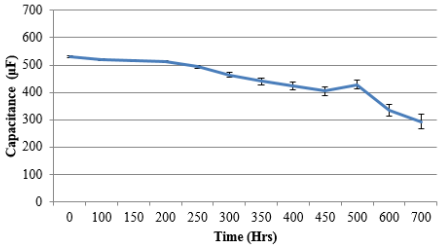

Capacitance – TH 270µF

K- M5 270µF/16V

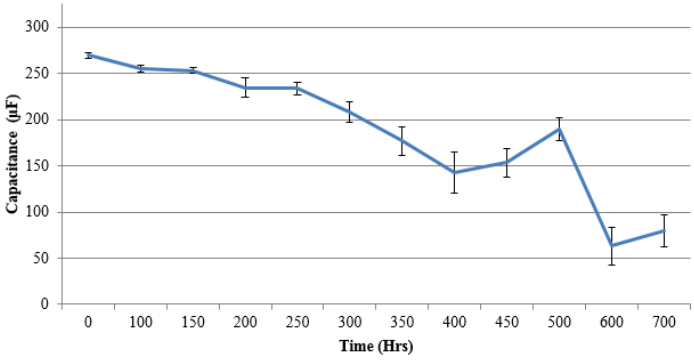

Capacitance – TH 100µF

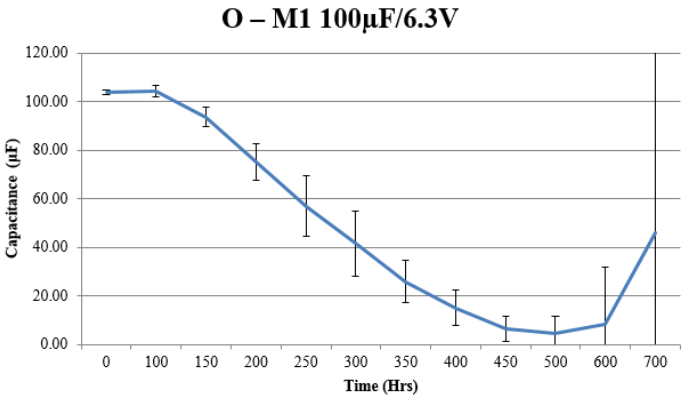

Capacitance – TH 470µF

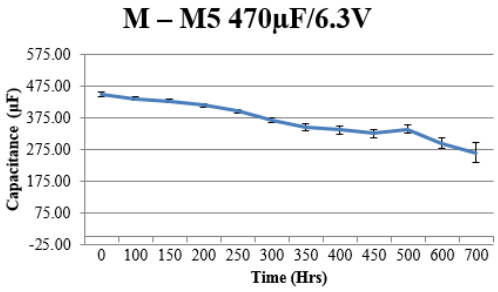

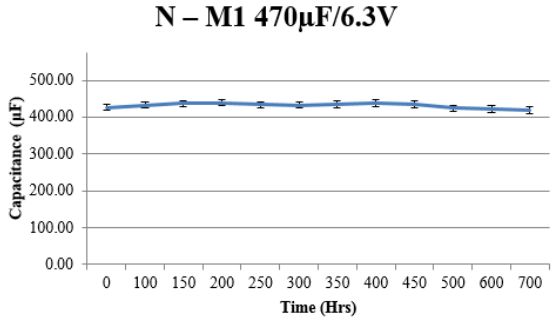

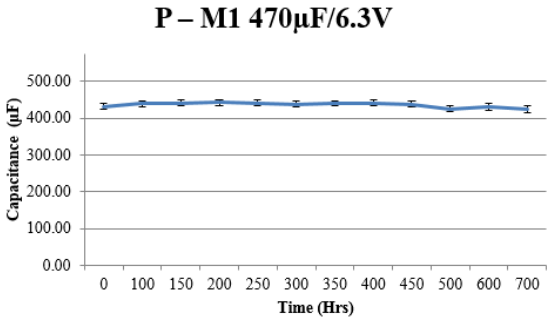

1. Dissipation Factor Results

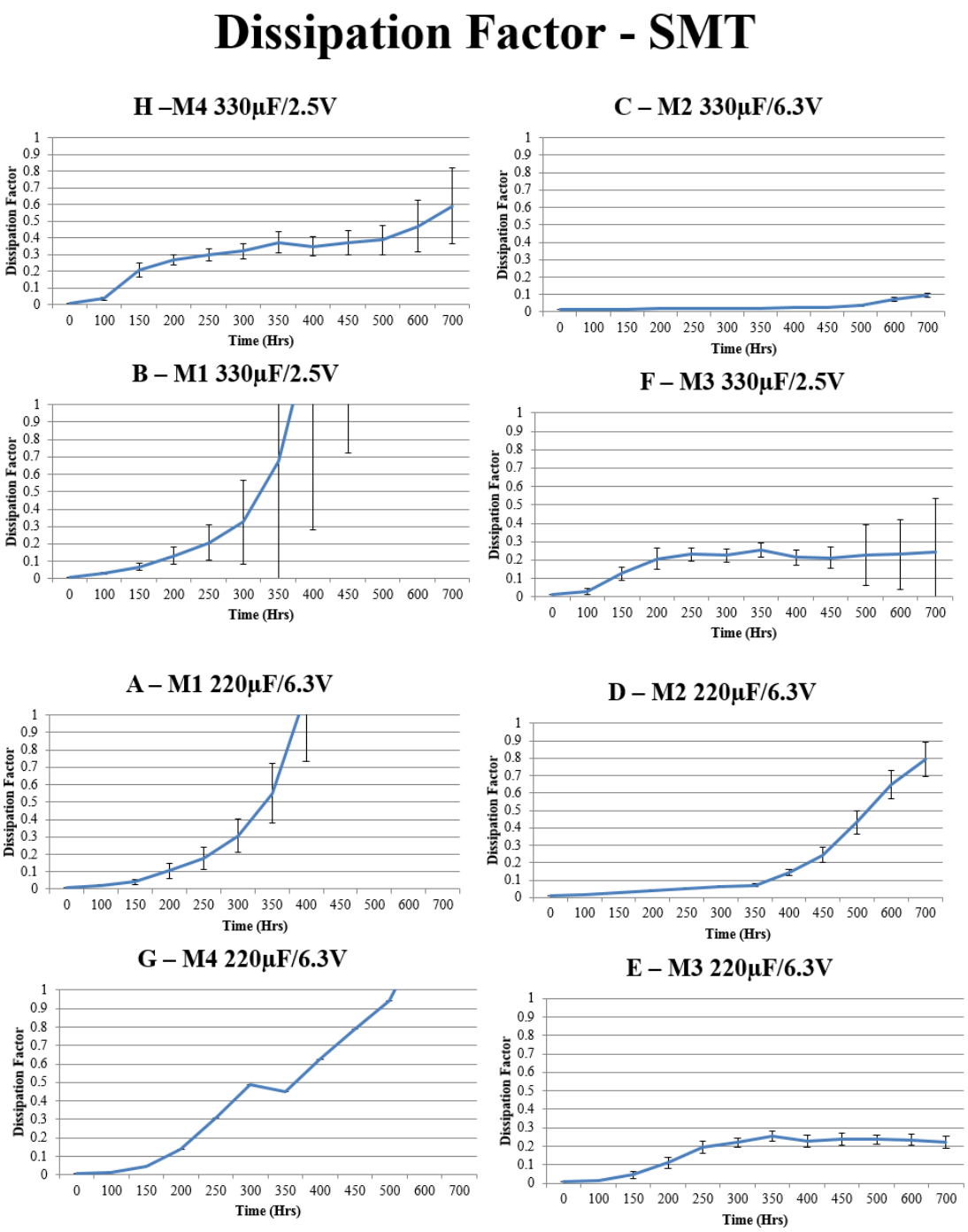

Dissipation Factor – THT

I – M5 560µF/6.3V

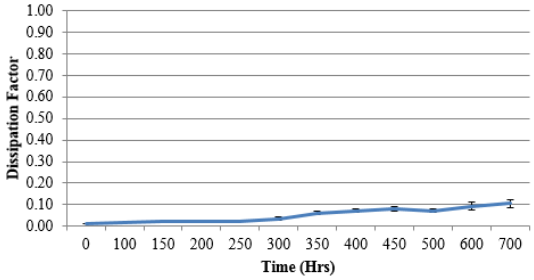

L – M5 560µF/6.3V

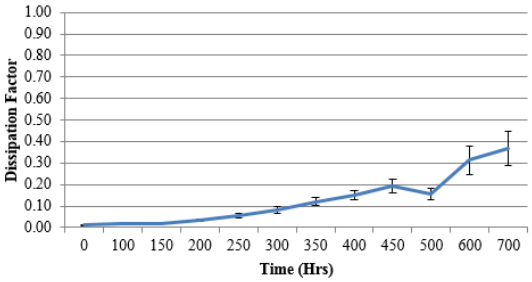

J – M5 560µF/6.3V

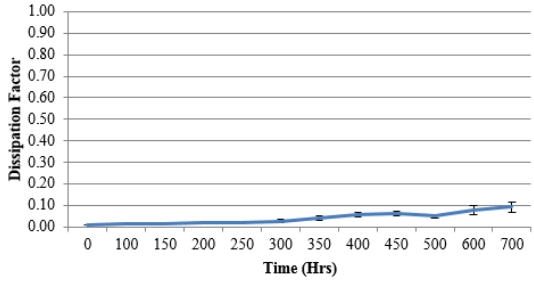

K- M5 270µF/16V

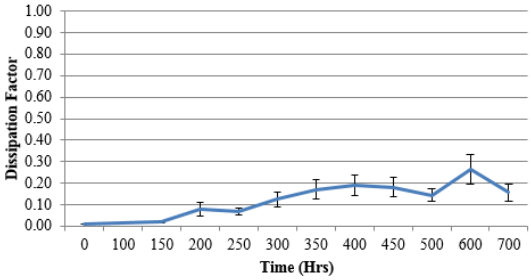

M – M5 470µF/6.3V

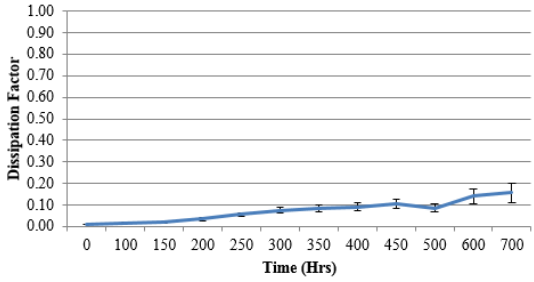

O – M1 470µF/6.3V

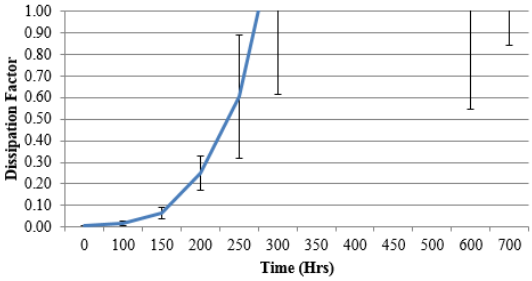

N – M1 470µF/6.3V

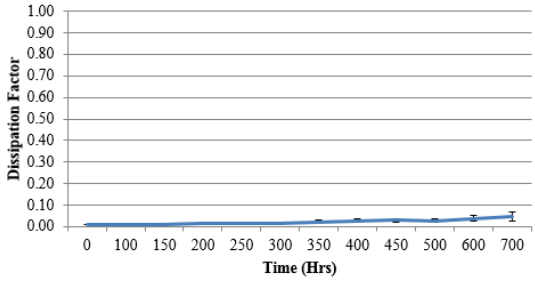

P – M1 470µF/6.3V

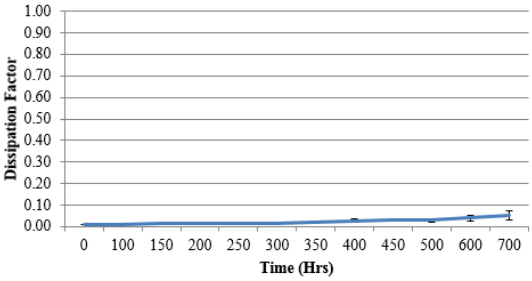

2. Equivalent Series Resistance Results

ESR - SMT

A – M1 220µF/6.3V

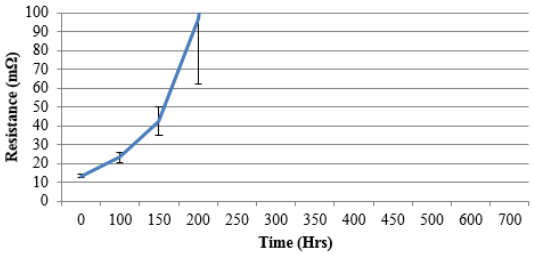

E – M3 220µF/6.3V

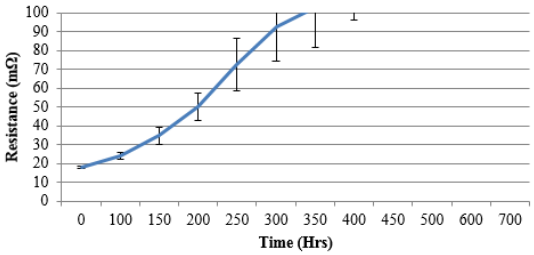

G – M4 220µF/6.3V

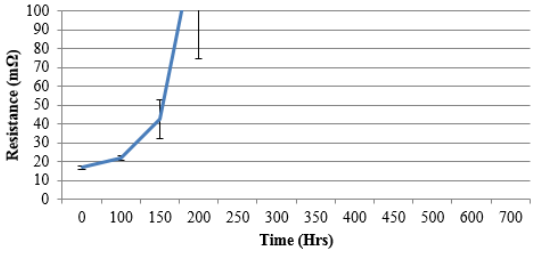

D – M2 220µF/6.3V

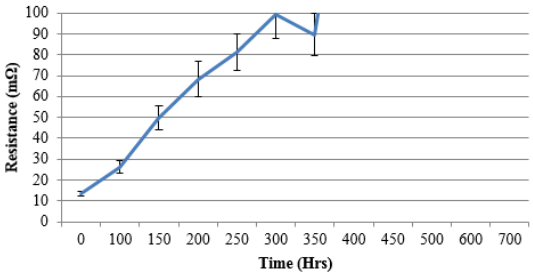

B – M1 330µF/2.5V

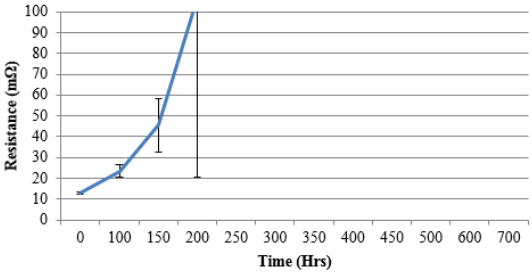

C – M2 330µF/6.3V

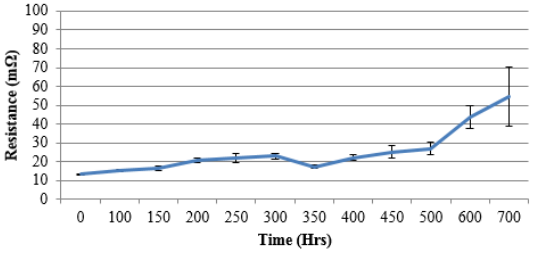

F – M3 330µF/2.5V

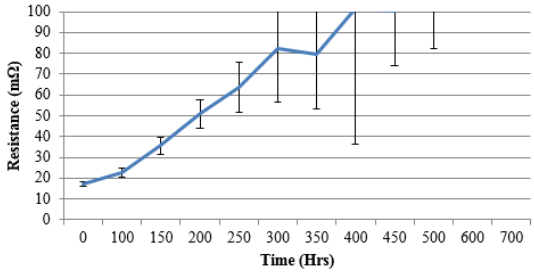

H –M4 330µF/2.5V

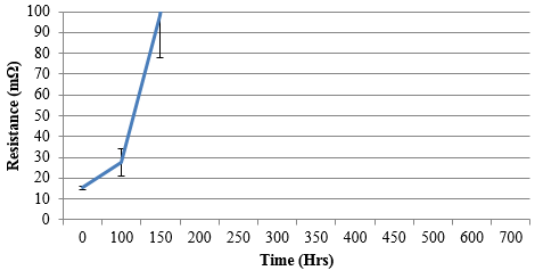

ESR – TH

I – M5 560µF/6.3V

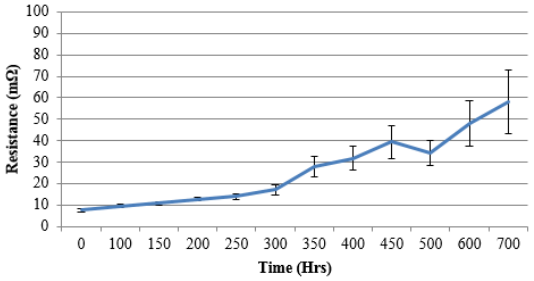

L – M5 560µF/6.3V

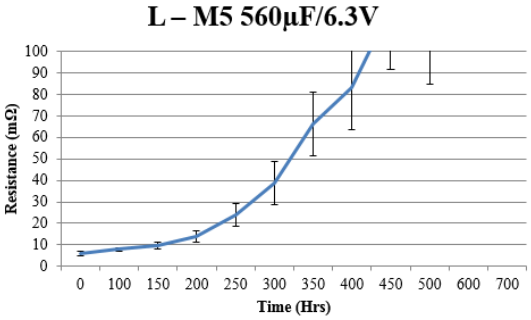

J – M5 560µF/6.3V

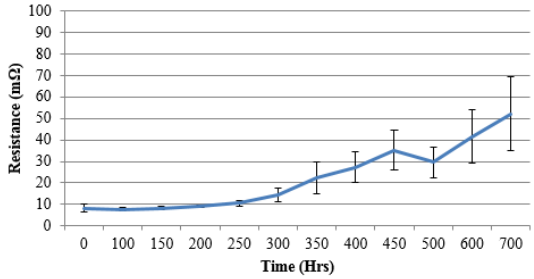

K- M5 270µF/16V

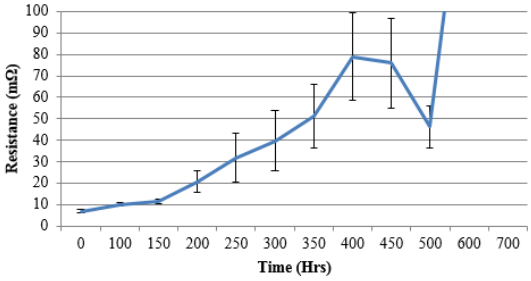

M – M5 470µF/6.3V

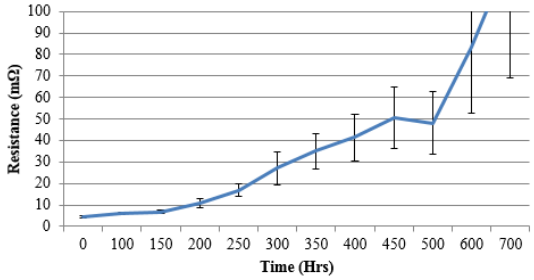

O – M1 470µF/6.3V

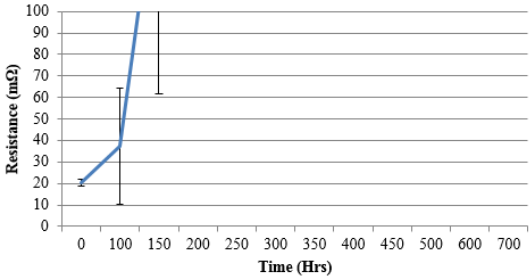

N – M1 470µF/6.3V

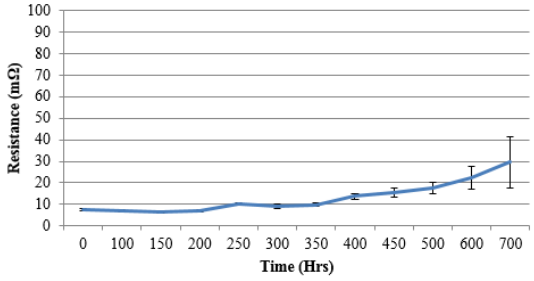

P – M1 470µF/6.3V

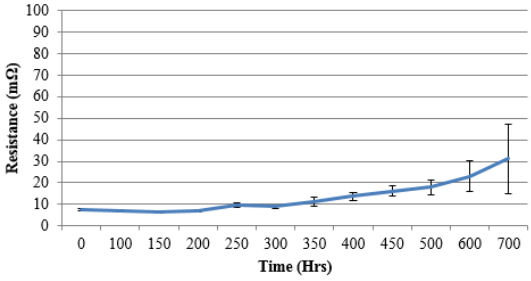

3. Leakage Current Results

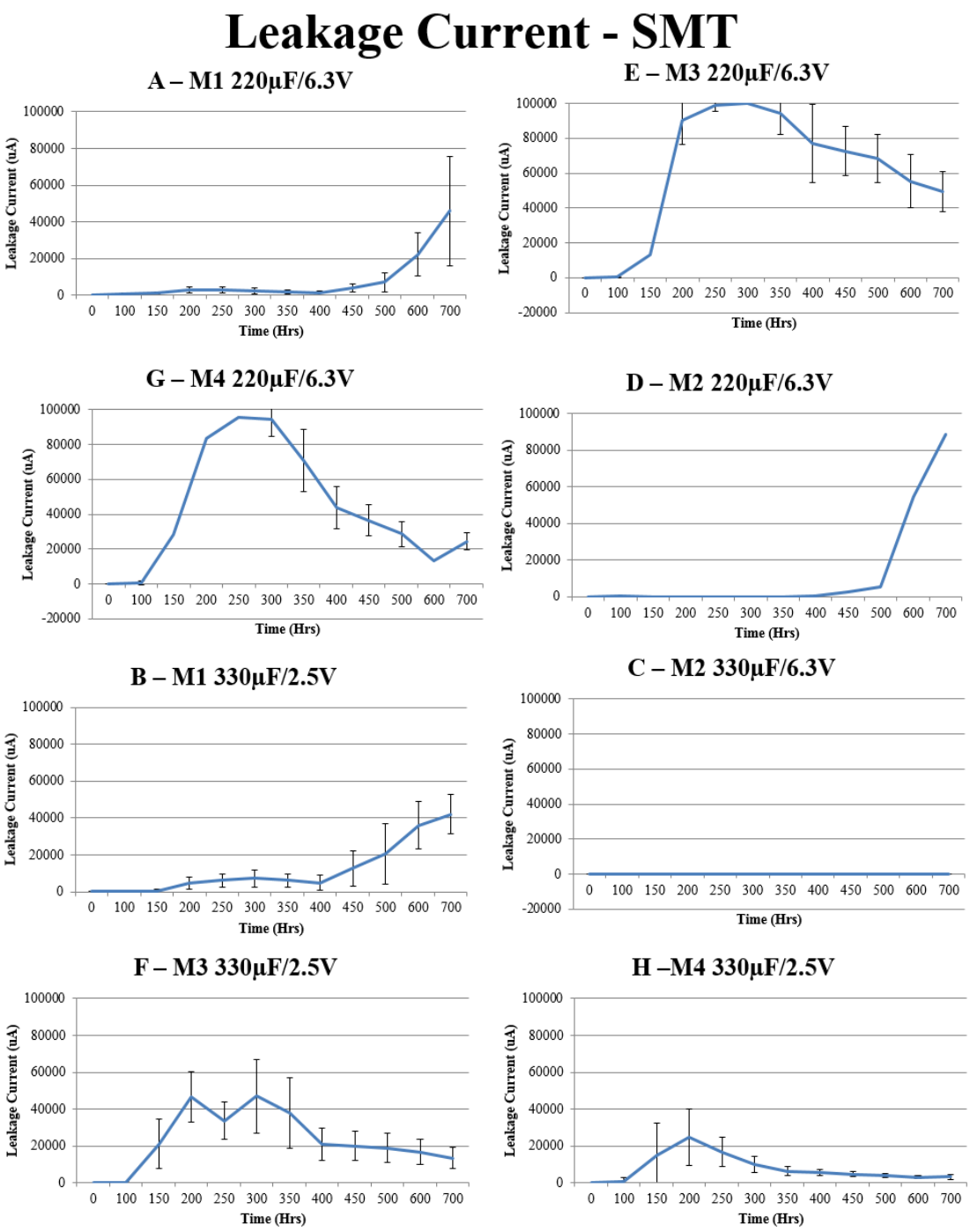

Leakage Current – TH

I – M5 560µF/6.3V

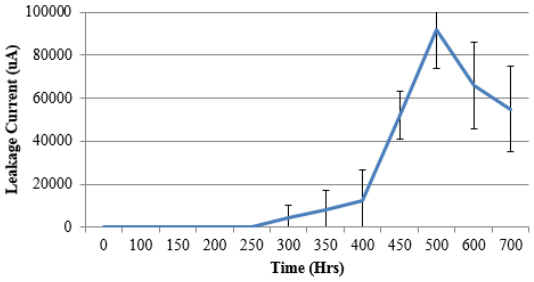

K- M5 270µF/16V

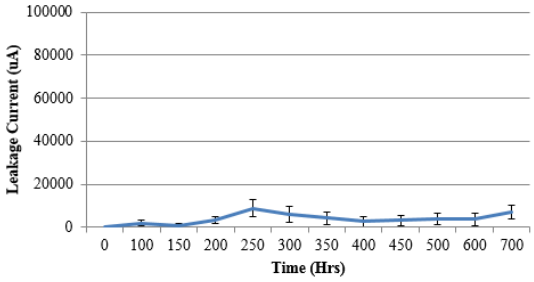

J – M5 560µF/6.3V

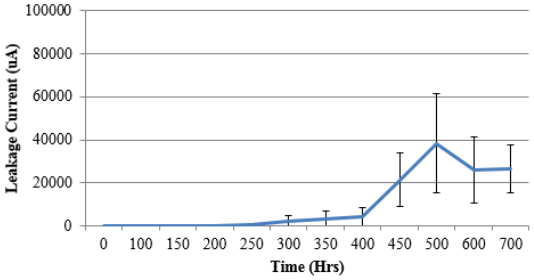

L – M5 560µF/6.3V

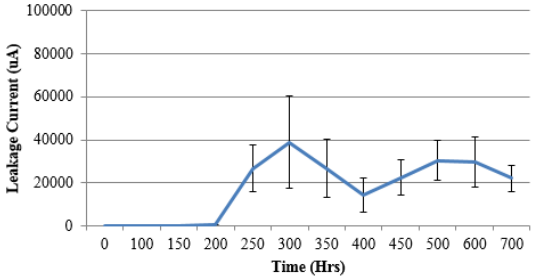

M – M5 470µF/6.3V

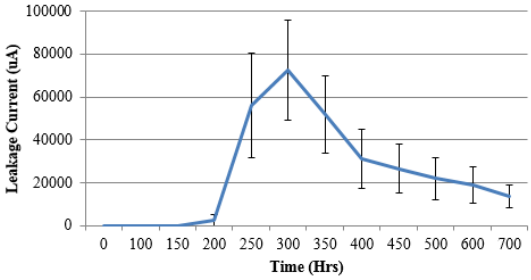

O – M1 470µF/6.3V

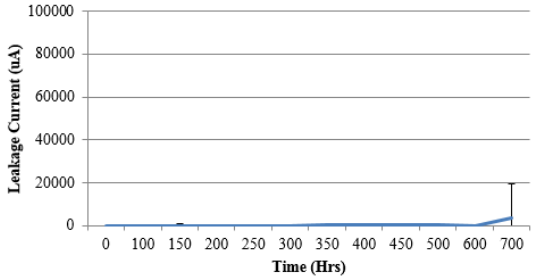

N – M1 470µF/6.3V

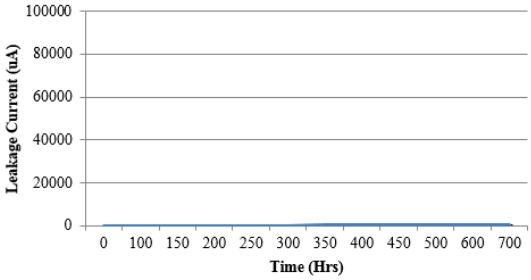

P – M1 470µF/6.3V

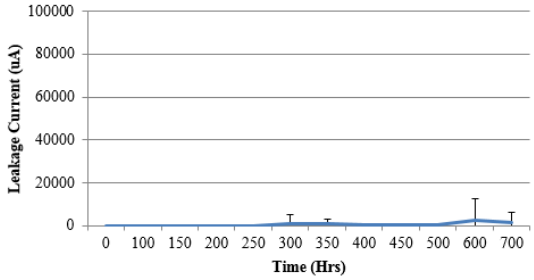

Appendix B – Results from Geometry-Based HAST Testing

1. Capacitance Results

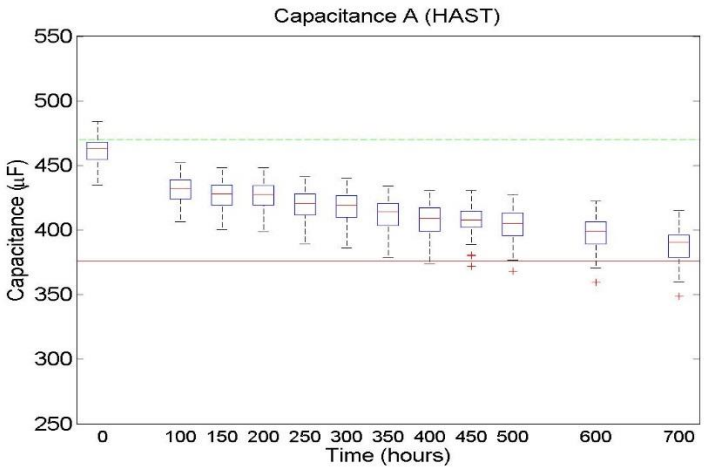

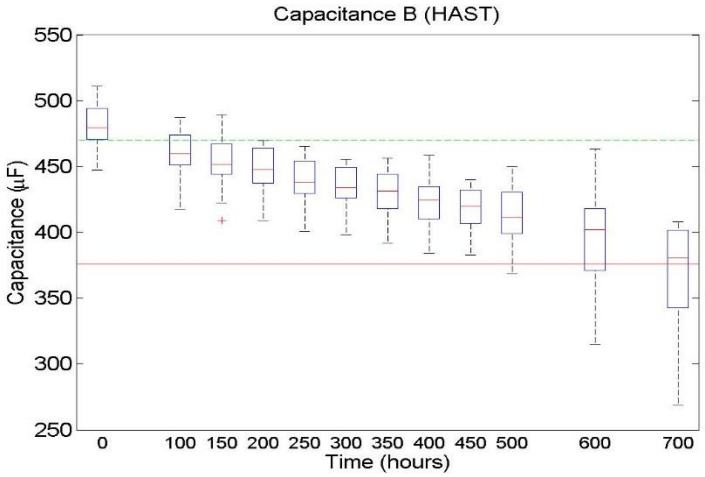

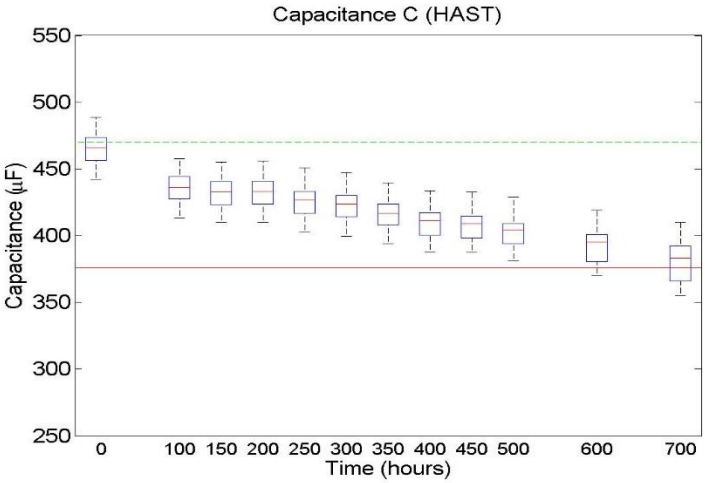

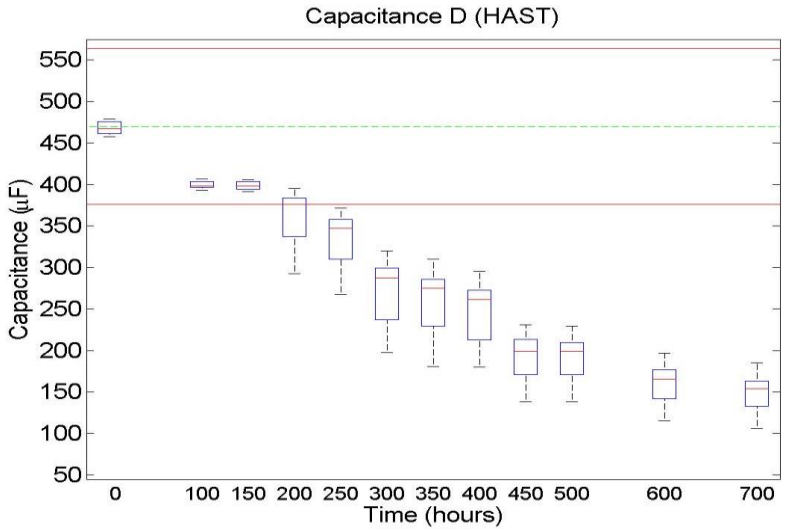
Capacitance D (HAST)
Capacitance (µF)
550
500
450
400
350
300
250
200
150
100
50
0
100 150 200 250 300 350 400 450 500
600
700
Time (hours)

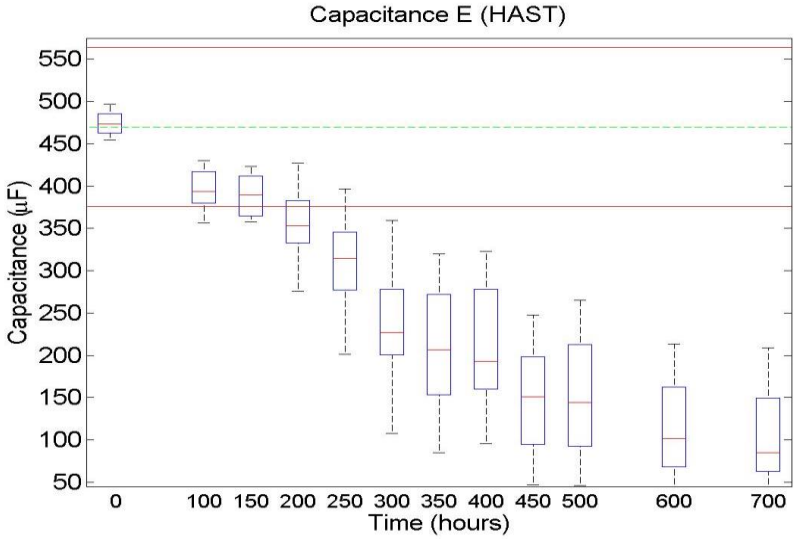
Capacitance E (HAST)
Capacitance (µF)
550
500
450
400
350
300
250
200
150
100
50
0
100 150 200 250 300 350 400 450 500
600
700
Time (hours)

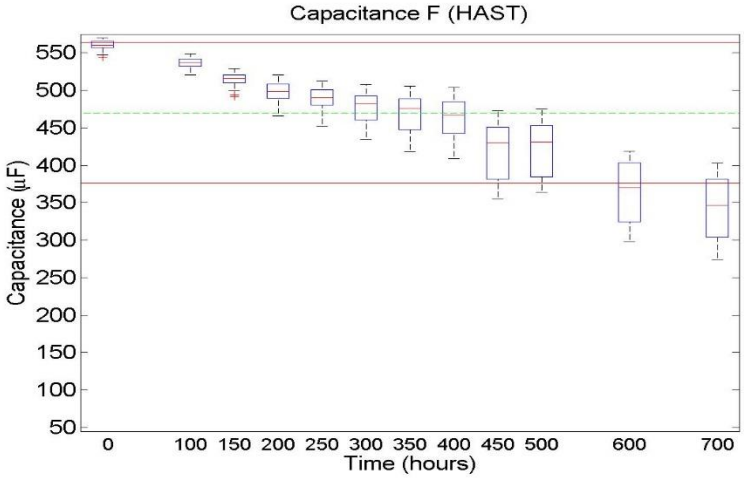
Capacitance F (HAST)
Capacitance (µF)
550
500
450
400
350
300
250
200
150
100
50
0
100 150 200 250 300 350 400 450 500
600
700
Time (hours)

2. Dissipation Factor Results

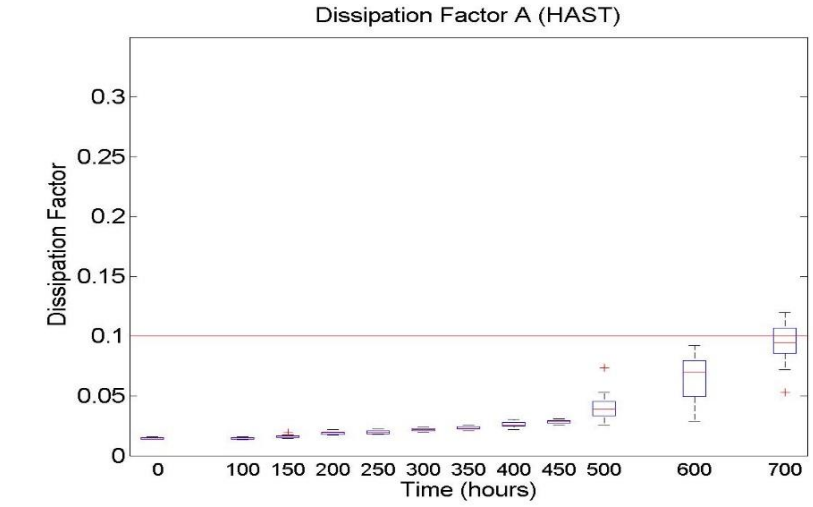

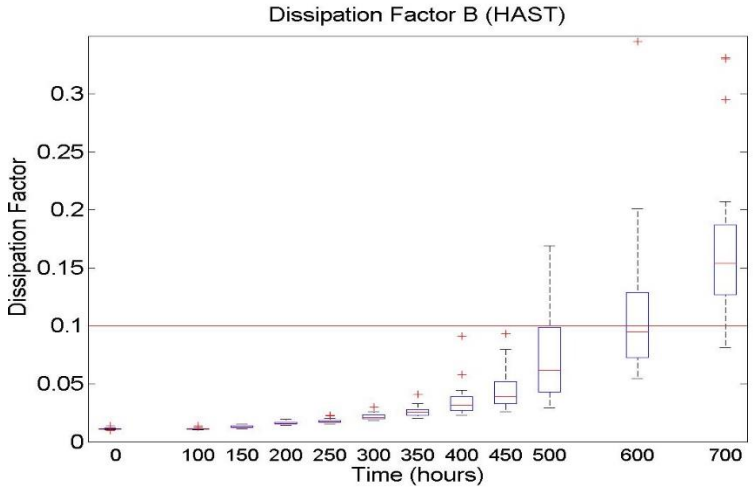

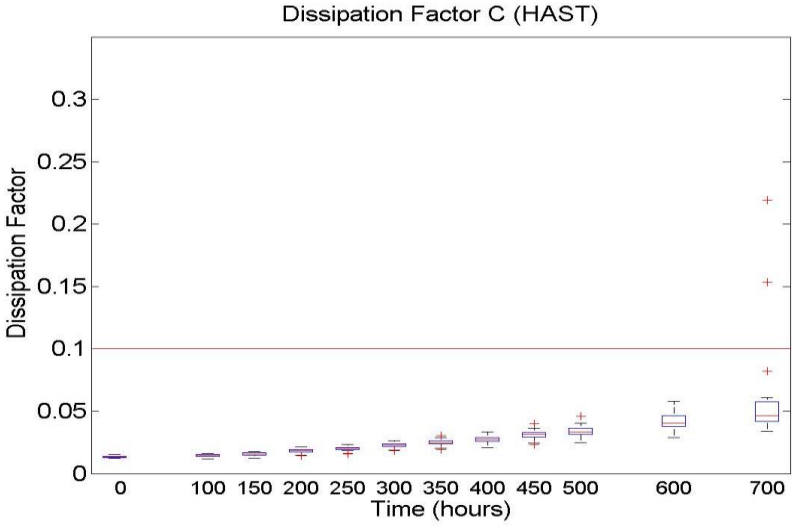

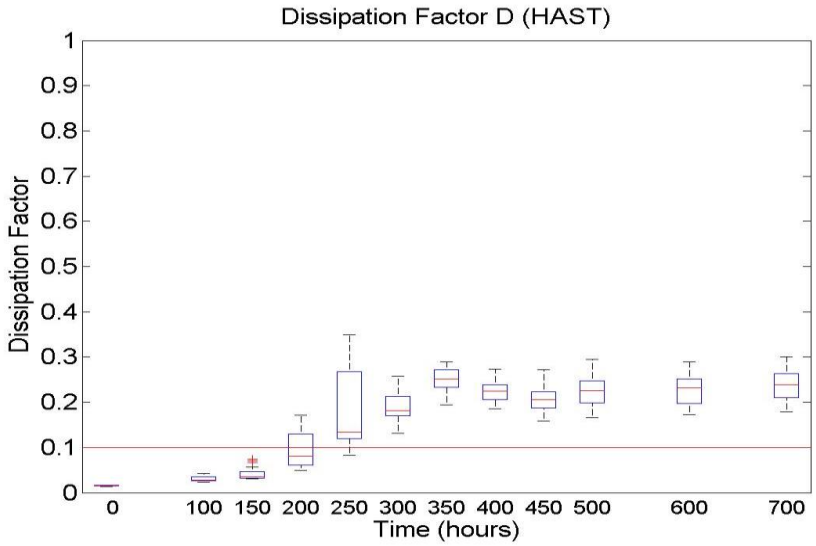
Dissipation Factor D (HAST)
Dissipation Factor
Time (hours)
0
0.1
0.2
0.3
0.4
0.5
0.6
0.7
0.8
0.9
1
0
100
150
200
250
300
350
400
450
500
600
700

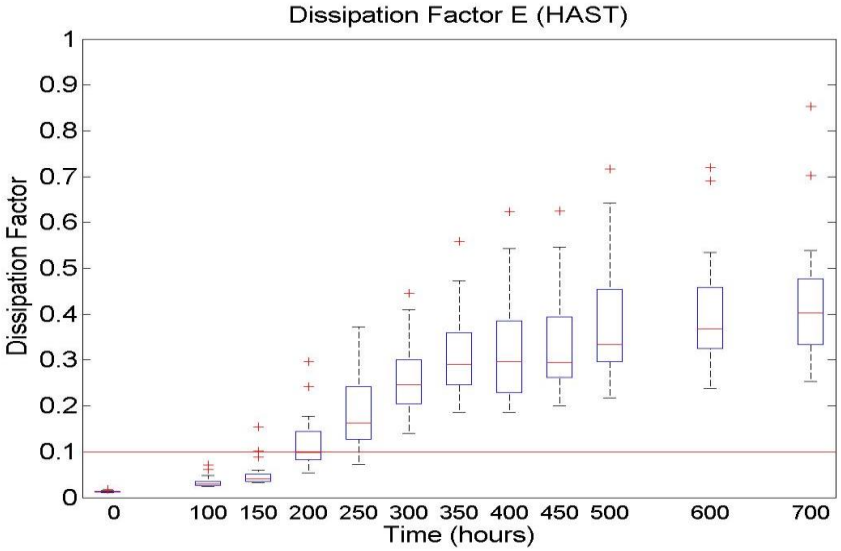
Dissipation Factor E (HAST)
Dissipation Factor
Time (hours)
0
0.1
0.2
0.3
0.4
0.5
0.6
0.7
0.8
0.9
1
0
100
150
200
250
300
350
400
450
500
600
700

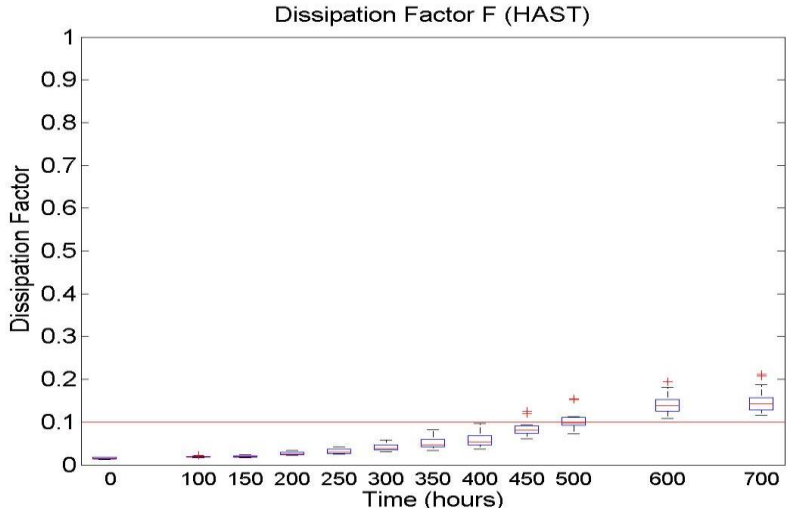
Dissipation Factor F (HAST)
Dissipation Factor
Time (hours)
0
0.1
0.2
0.3
0.4
0.5
0.6
0.7
0.8
0.9
1
0
100
150
200
250
300
350
400
450
500
600
700

3. Equivalent Series Resistance Results

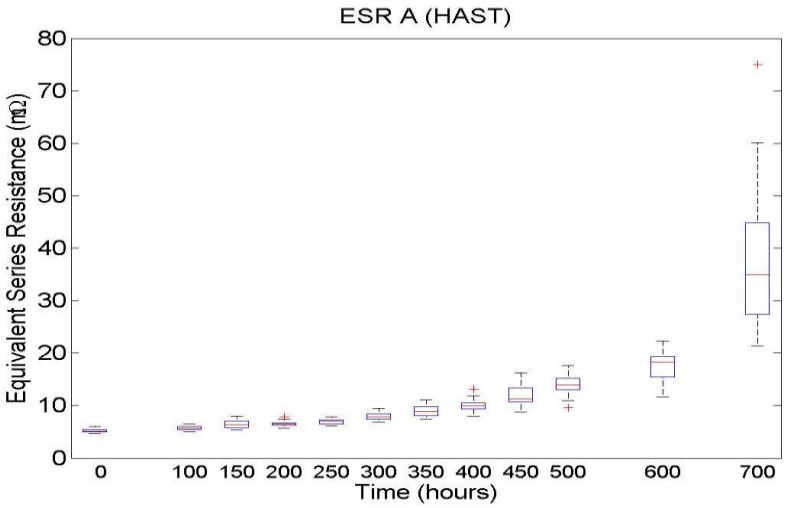

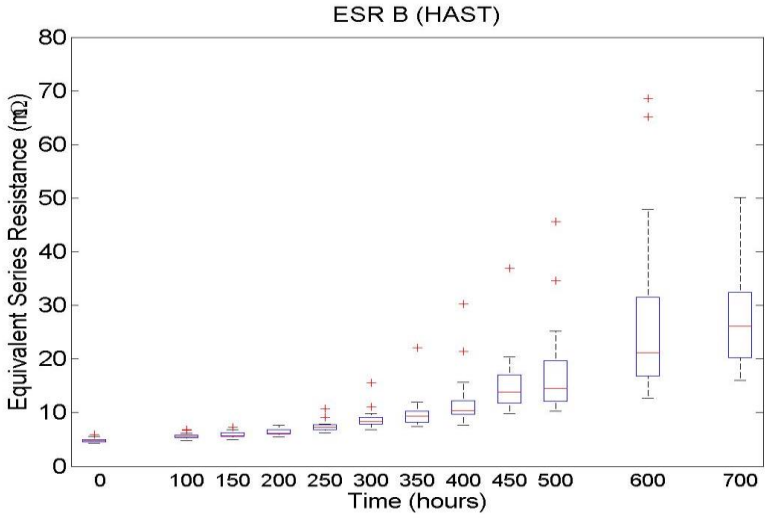

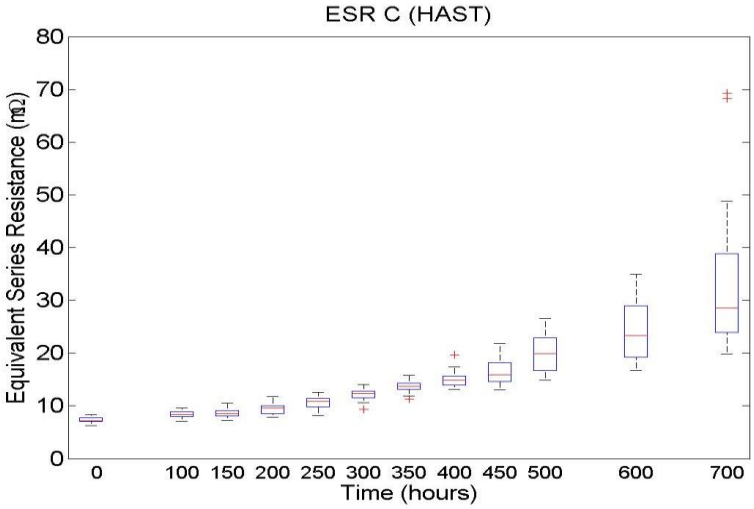

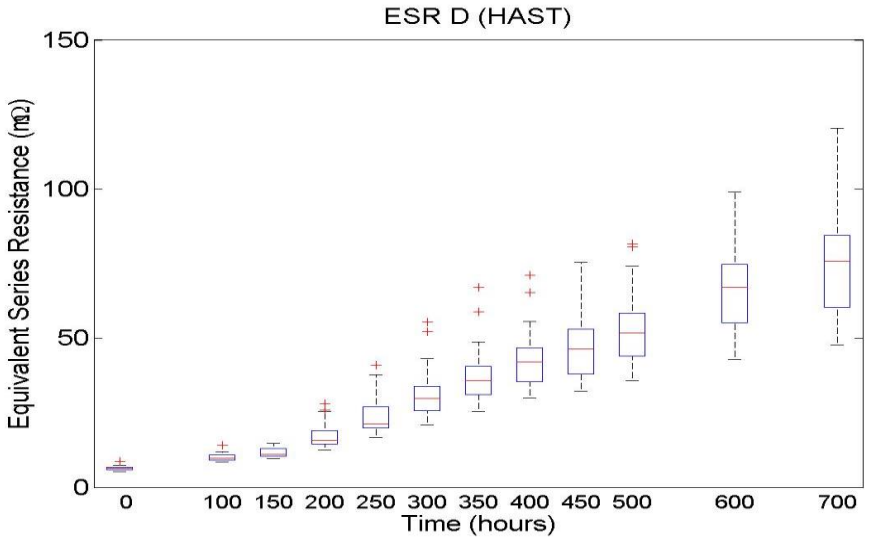
ESR D (HAST)
Equivalent Series Resistance (mΩ)
150
100
50
0
0
100
150
200
250
300
350
400
450
500
600
700
Time (hours)

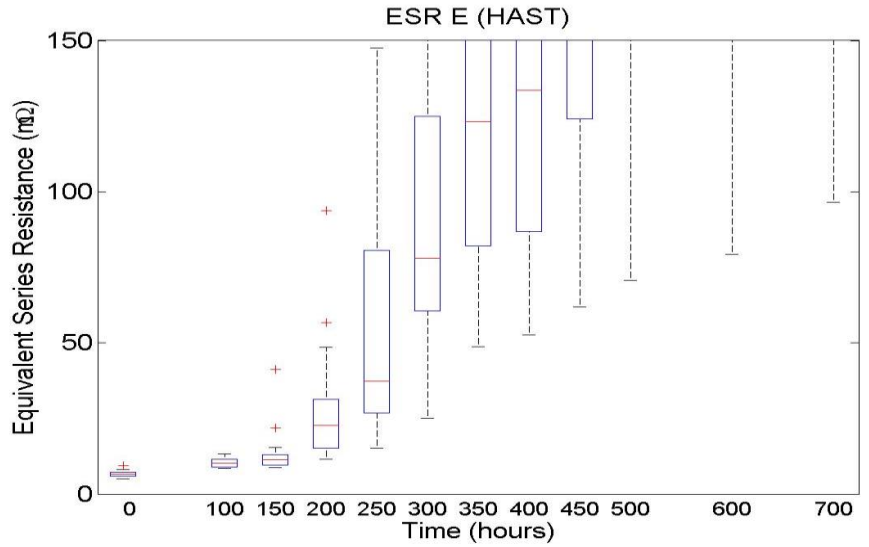
ESR E (HAST)
Equivalent Series Resistance (mΩ)
150
100
50
0
0
100
150
200
250
300
350
400
450
500
600
700
Time (hours)

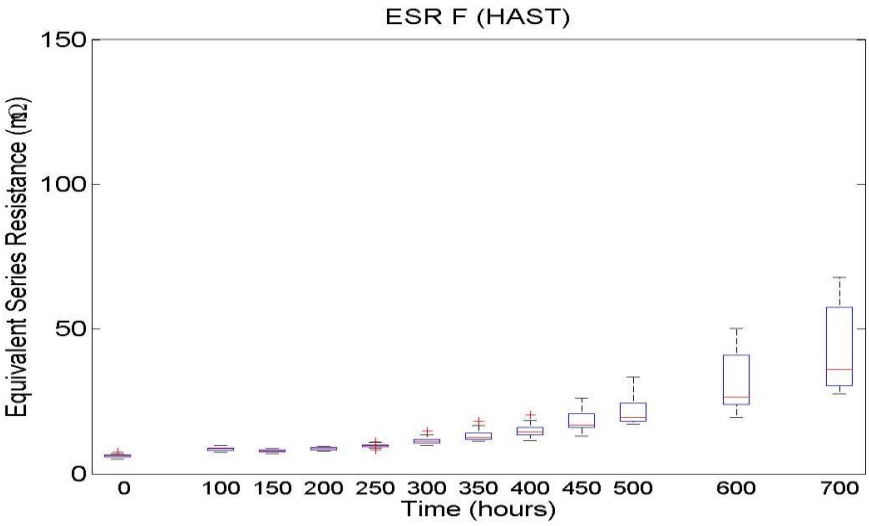
ESR F (HAST)
Equivalent Series Resistance (mΩ)
150
100
50
0
0
100
150
200
250
300
350
400
450
500
600
700
Time (hours)

4. Leakage Current Results

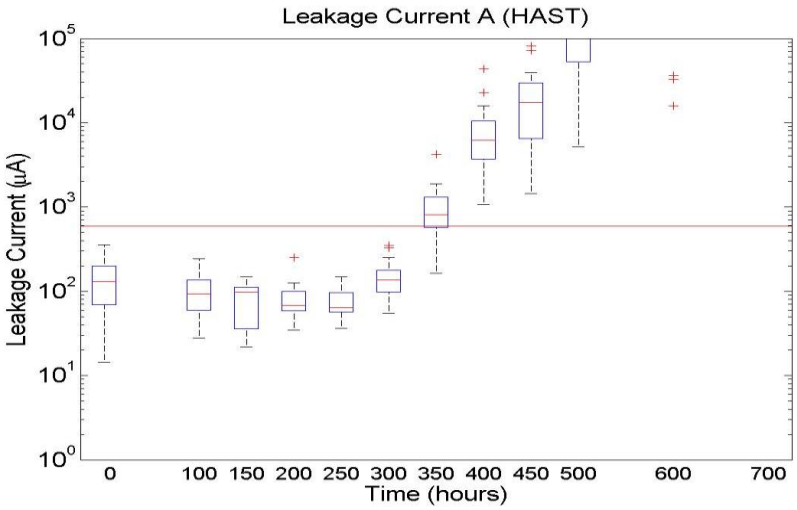

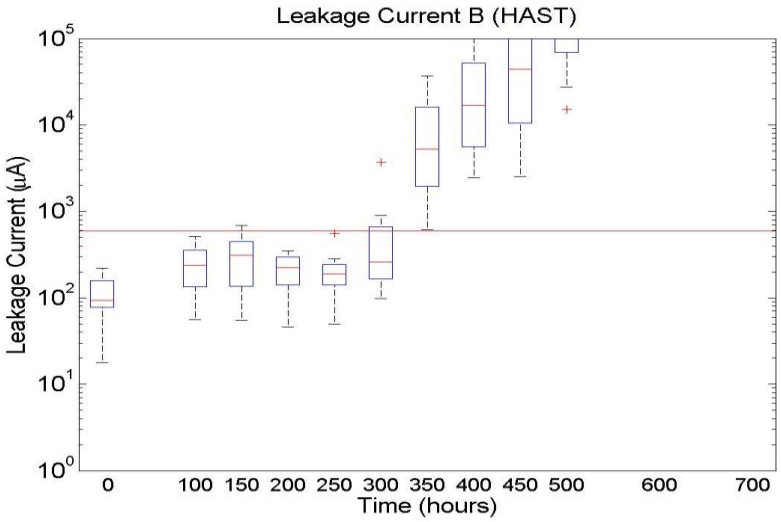

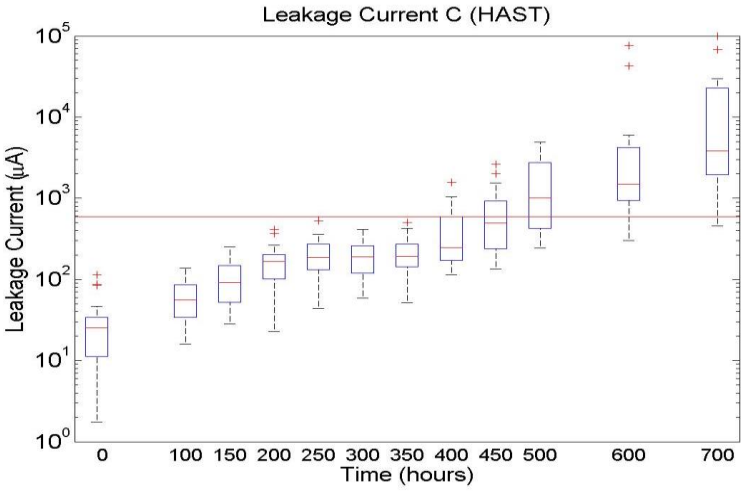

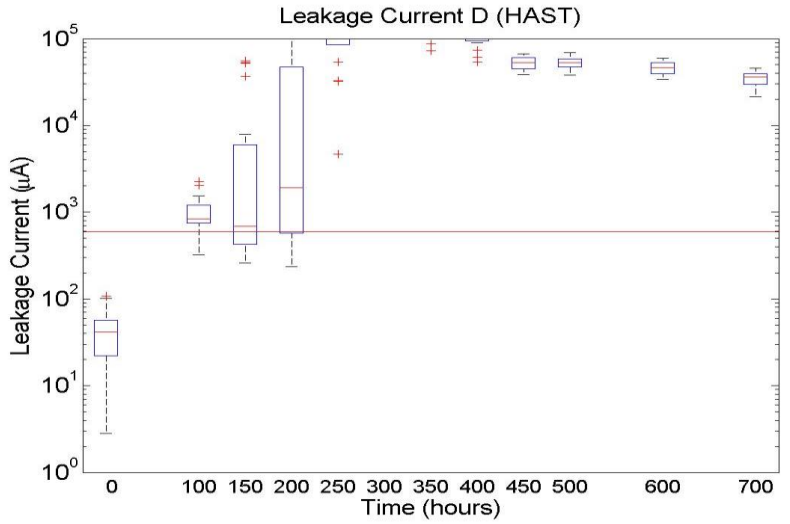
Leakage Current D (HAST)
Leakage Current (µA)
10^0
10^1
10^2
10^3
10^4
10^5
0
100 150 200 250 300 350 400 450 500
600
700
Time (hours)

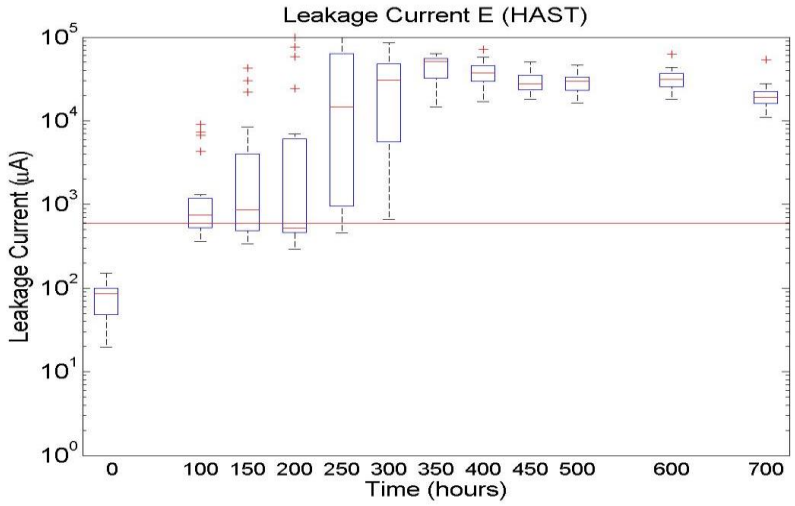
Leakage Current E (HAST)
Leakage Current (µA)
10^0
10^1
10^2
10^3
10^4
10^5
0
100 150 200 250 300 350 400 450 500
600
700
Time (hours)

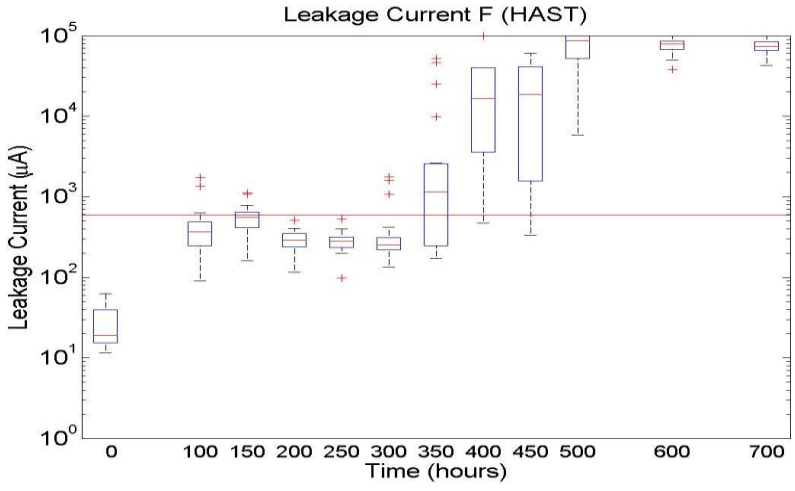
Leakage Current F (HAST)
Leakage Current (µA)
10^0
10^1
10^2
10^3
10^4
10^5
0
100 150 200 250 300 350 400 450 500
600
700
Time (hours)

References

[1] R. Deshpande, Capacitors Technology and Trends, vol. 1, New Delhi: Tata McGraw-Hill, 2012.

[2] W. Sarjeant, J. Zirnheld and F. MacDougall, "Capacitors," *IEEE Transactions on Plasma Science,* vol. 26, no. 5, pp. 1367-1392, 1998.

[3] Nichicon Corporation, "Latest Technological Trends for Conductive Polymer Aluminum Solid Electrolytic Capacitors," [Online]. Available: www.digikey.com. [Accessed 3 March 2016].

[4] A. Elschner, S. Kirchmeyer, W. Loevenich, U. Merker and K. Reuter, PEDOT Principles and Applications of an Intrinsically Conductive Polymer, Boca Raton, Florida: CRC Press, 2011.

[5] Heraeus, "Clevios Conductive Polymers," Heraeus, 2014. [Online]. Available: www.heraeus-clevios.com. [Accessed 20 November 2014].

[6] M. Kim, J. Yoo, H. Im and J. Kim, "The Effects of Different Oxidants on the Characteristics of Conductive Polymer Aluminum Solid Electrolyte Capacitors," *Journal of Power Sources,* vol. 230, pp. 1-9, 2013.

[7] K. Nogami, K. Sakamoto, T. Hayakawa and M. Kakimoto, "The Effects of Hyperbranched Poly(siloxysilane)s on Conductive Polymer Aluminum Solid Electrolytic Capacitors," *Journal Of Power Sources,* vol. 166, no. 2, pp. 584-589, 2007.

[8] Rubycon Corporation, "Manufacture of Aluminum Electrolytic Capacitors," [Online]. Available: www.rubycon.co.jp. [Accessed 11 February 2016].

[9] Panasonic Industrial, "Conductive Polymer Aluminum Solid Capacitors (OS-CON)," 2016. [Online]. Available: https://industrial.panasonic.com. [Accessed 11 February 2016].

[10] Paumanok Publications, Inc., "Polymer Aluminum Capacitors World Markets, Technologies & Opportunities: 2012-2017," Paumanok Publications Inc,, Cary, 2016.

[11] Nippon Chemi-con Corporation, "Conductive Polymer Aluminum Solid Capacitors, Application Note," 2009. [Online]. Available: http://www.chemi-con.co.jp/e/catalog/pdf/Application_Note_NPCAP_090716e.pdf. [Accessed 10 January 2015].

[12] D. Liu, "Physical and Electrical Characterization of Aluminum Polymer Capacitors," National Aeronautics and Space Administration, Greenbelt, 2009.

[13] Rubycon, "Conductive Polymer Aluminum Electrolytic Capacitors "PZ-CAP" Introduction," 30 January 2013. [Online]. Available: http://www.rubycon.co.jp/en/products/. [Accessed 20 February 2016].

[14] T. Zednicek and J. Gill, "Voltage Derating Rules for Solid Tantalum and Niobium Capacitors," in *CARTS Europe 2003*, 2003.

[15] Cornell Dubilier, "Aluminum Electrolytic Capacitor Application Notes," 2016. [Online]. Available: www.cde.com/resources/catalogs/AEappGUIDE.pfg. [Accessed 11 February 2016].

[16] R. Alwitt and H. Uchi, "Electrochemical Tunnel Etching of Aluminum," *Journal of The Electrochemical Society,* vol. 131, no. 1, pp. 13-17, 1984.

[17] M. Hunter and P. Fowle, "Natural and Thermally Formed Oxide Films on Aluminum," *Journal of the Electrochemical Society,* pp. 482-485, 1956.

[18] L. Macomber and J. Rapoza, "Solid Polymer Aluminum Capacitor Chips in DC-DC Converter Modules Reduce Cost and Size and Improve High-Frequency Performance," in *International PCIM 2001 Power Electronics Conference*, Rosemont, 2001.

[19] Murata, "Polymer Aluminum Electrolytic Capacitors," 2014. [Online]. Available: www.murata.com. [Accessed 11 February 2016].

[20] Vishay, "General Information and Specifications Conductive Polymer Capacitors," 2015. [Online]. Available: www.vishay.com/docs. [Accessed 20 February 2016].

[21] Manyue, "Conductive Polymer Aluminum Solid Capacitors," [Online]. Available: www.manyue.com/xcon_application.pdf. [Accessed 20 January 2016].

[22] M. Kus and S. Okur, "Electrical Characterization of PEDOT:PSS Beyond Humidity Saturation," *Sensors and Actuators B: Chemical,* vol. 143, no. 1, pp. 177-181, 2009.

[23] H. Kang, J. Lee, J. Joo, J. Ko, M. Kim and J. Lee, "Humidity-Dependent Characteristics of Thin Film Poly(3,4-ethylenedioxythiophene) Field-Effect Transistor," *Synthetic Metals,* vol. 155, no. 1, pp. 176-179, 2005.

[24] A. Shrivastava, "Reliability Evaluation of Liquid and Polymer Aluminum Electrolytic Capacitors , ph.d Thesis," Digital Repository at the University of Maryland , College Park, 2014.

[25] N. W., Accelerated Testing; Statistical Models, Test Plans and Data Analyses, New York: Wiley, 1990.

[26] S. Sakamoto, M. Okumura, Z. Zhao and Y. Furukawa, "Raman Spectral Changes of PEDOT-PSS in Polymer Light-Emitting Diodes Upon Operation," *Chemical Physics Letters*, vol. 412, no. 4-6, pp. 395-398, 2005.

[27] W. Chiu and J. Travas-Sejdic, "Studies of Dopant Effects in Poly(3,4-ethylenedioxythiophene) Using Raman Spectroscopy," *Journal of Raman Spectroscopy,* vol. 37, no. 12, pp. 1354-1361, 2006.

[28] W. W. Chiu and J. Travas-Sedjdic, "Spectroscopic and Conductivity Studies of Doping in Chemically Synthesized Poly(3,4-ethylenedioxythiophene)," *Synthetic Metals,* vol. 155, no. 1, pp. 80-88, 2005.

[29] Renishaw, "Raman Spectra Explained," 2014. [Online]. [Accessed 15 November 2014].

[30] N. Colthup and L. H. Daly, Introduction to Infrared and Raman Spectroscopy, New York: Academic Press, 1975.

[31] A. Shrivastava, *Reliability Evaluation of Liquid and Polymer Aluminum Electrolytic Capacitors,* College Park: University of Maryland, 2014.

[32] M. Hunter and P. Fowle, "Natural and Thermally Formed Oxide Films on Aluminum," *Journal of the Electrochemical Society,* vol. 103, no. 9, p. 482, 1956.